Volume 7 MAY, 1936 Number 5

PHYSICS

A Journal of General and Applied Physics

VIII. The Correlation of the Distillation Range with the Penetration of Creosote into Paper Strips*

C. J. FROSCH, *Bell Telephone Laboratories, Inc.*

(Received February 17, 1936)

Measurements of the penetration tensions in paper of a series of creosotes distilled from a single coal tar are reported (the penetration tension being the product of the surface tension and the cosine of the contact angle). It is found that these data conform to two equations: one, previously developed by others from theoretical considerations of the effects of variation in size and distribution of capillary pores upon the theoretical equation of flow, the other, an empirical relationship which is less difficult to apply in more practical problems where many data must be analyzed. The creosote-paper contact angles are shown to be zero or extremely small. Possible errors in the paper strip method are discussed and the importance of calibrating each strip with a reference liquid is demonstrated. The failure of Washburn's equation, which has received considerable attention in the field of fibrous penetration, is shown to be due to the neglect of the hydrostatic head term. The penetration tensions of these creosotes are unaltered by the presence of adsorbed water.

INTRODUCTION

WHILE industry has long been fully cognizant of the commercial importance of solid-liquid relations in the various processes of manufacture which depend upon the movement of liquid penetrants in fibrous materials, the laws governing the dynamics of liquid flow in such materials are still in the early stages of development. This has not been due to a lack of research on the subject but rather to the inherent difficulties encountered in a study of this nature. As examples of such difficulties may be cited the inability to duplicate samples; variations in the size, shape and distribution of the capillary pores; moisture effects; possible swelling brought about by the adsorption of the liquid penetrant; visual difficulties and a lack of knowledge of the specific mutual relations at solid-liquid interfaces. As a consequence, the equations of flow in fibrous materials have more generally been derived from a consideration of liquid flow in uniform capillaries.

The most direct method which has been employed to study the penetration of liquids in nonuniform capillary systems is known as the Klemm test. It depends upon the fact that wetting liquids, due to capillarity, will rise in strips of a fibrous material when one end of the strip is brought in contact with a liquid.

Impregnation of wood is the fundamental concern of this investigation but the difficulties involved in the preparation and study of thin uniform strips of wood suggested the substitution of a more convenient fibrous material. The somewhat similar composition and structure that exists in paper and wood encouraged the belief that useful information could be obtained by a study of the penetration of creosote into paper strips.

The eight creosotes of the Fulweiler series were selected as penetrants since the necessary physical constants had already been determined.[1] These creosotes were all distilled from a common tar but differed in volatility because of variations in the temperature of distillation.

* This paper is one of a series entitled "Chemical Studies of Wood Preservation" being published in this journal and in Industrial and Engineering Chemistry.

[1] Frosch, Physics **6**, 165 (1935).

Historical

The dynamic movement of liquids in capillary systems such as soil and blotting paper was considered by Bell and Cameron.[2] They showed that the penetration could be expressed by the empirical relation.

$$h^n = kt, \tag{1}$$

in which t is the time required to penetrate the structure to a height h and n and k are constants. They found the value of n to be 2.3.

Later Ostwald[3] deduced the equivalent equation

$$h = kt^n, \tag{2}$$

which Lucas[4] applied to the rise of various liquids in filter paper and found values of n ranging from 0.424 to 0.500 corresponding to exponents of 2.00 to 2.36 in Eq. (1). Simmonds[5] arrived at a value of n equal to 0.425 for the penetration of water into blotting paper, cardboard and unbeaten sulphite pulp.

More recently Washburn[6] considered the penetration of liquids in uniform capillaries. He showed that inertia effects are inappreciable after the penetration has progressed a measurable distance and, for small capillaries, may be neglected. He also considered hydrostatic effects but suggested that these may be neglected in comparison with capillary forces when dealing with small capillaries. His equation then takes the form

$$h^2 = rt\gamma \cos \theta / 2\eta; \tag{3}$$

neglecting the viscosity of the displaced gas, where γ is the surface tension of the liquid, η is the viscosity, r the radius of the capillary and θ is the angle of contact between the liquid and the solid. Whitehead and Greenfield[7] applied this equation to the capillary rise of oils in cable insulation papers and found that a particular value of r for each paper satisfies the penetration data.

Peek and McLean[8] have shown that while the effect of hydrostatic head may be small, it is not always insignificant even for the penetration of liquids into small capillaries. They considered not only the effects of hydrostatic head in their study but also the effects of variations in size and distribution of pores upon the theoretical equation of flow for uniform capillaries. They derived an equation in the form

$$\frac{dh}{dt} = \frac{A\gamma \cos \theta}{4\eta h} - \frac{Bdg}{8\eta}, \tag{4}$$

where A and B are constants for each paper strip depending upon the pore size distribution function. They have shown that B will be equal to A^2 only for the case of uniform capillary pores throughout the paper structure when A becomes analogous to r in Eq. (3). The application of Eq. (4) to experimental data is by graphic means.

Fibrous Penetration

The kinetics of flow involved in the capillary rise of liquids in fibrous structures have already been considered by a great many investigators but will be briefly discussed here for the sake of completeness.

When a capillary of uniform radius r is brought in contact with a liquid which will wet it, the liquid will rise in the tube because of capillary pressure. This motion will be opposed by the hydrostatic head of the liquid so that the total force per unit cross section producing motion will be

$$2\gamma \cos \theta / r - hdg \tag{5}$$

for a vertical capillary. According to Poiseuille's law, the rate at which a liquid will penetrate a capillary, neglecting the viscosity of the displaced gas, is equal to

$$Pr^2 / 8\eta h, \tag{6}$$

where P is the total force producing motion. Substitution of the capillary tension and hydrostatic head forces for the value of P leads to a relationship very similar to Eq. (4). When the rate of flow is equal to zero, the equation has the

[2] Bell and Cameron, J. Phys. Chem. **10**, 658 (1906).
[3] Ostwald, Kolloid, Zeits. **2**, Suppl. No. 11 (1908).
[4] Lucas, Kolloid Zeits. **23**, 15 (1908).
[5] Simmonds, Paper Trade J. **97**, 40 (1933).
[6] Washburn, Phys. Rev. **17**, 273 (1921).
[7] Whitehead and Greenfield, Physics **3**, 324 (1932).
[8] Peek and McLean, Ind. Eng. Chem., Anal. Ed. **6**, 255 (1934).

form of Jurin's law which is used in a static method for the measurement of surface tension. The differential form of Eq. (3) results when the hydrostatic head of the liquid is neglected.

The penetration of a liquid in a paper strip is obviously more complex than that in uniform capillaries. The paths of liquid flow have become a maze of branching and connecting capillaries varying greatly in size throughout their length. Peek and McLean[8] considered the effects of variations in size and distribution of capillary pores upon the rate of penetration of liquids in paper strips. They assumed that the same distribution function of pore sizes holds throughout the length of the paper strips. Such an assumption is indeed reasonable when it is considered that the rate of liquid penetration in a given paper strip is substantially the same regardless of which end of the strip is submerged beneath the liquid. This obviously could not be the case unless the various pore sizes were distributed with substantially the same frequency throughout the paper. A constant distribution of pore sizes throughout the length of a paper strip requires a constant pore volume in any cross section of the paper. This seems to be indicated by the uniformity in density of small cross-sectional elements of a given paper strip.

It was in accordance with the above reasoning that Peek and McLean[8] deduced Eq. (4). They found that their equation gave a very good fit to their penetration data. They also found that A and B did not vary except for experimental error among all of the paper strips which they studied. It will be shown subsequently that A and B vary considerably among the paper strips considered herein but are essentially constant for a given paper strip when different liquids are employed. Since $A \cos\theta$ and B can be determined from a single penetration study, the problem resolves itself into the determination of A for each paper strip either by an independent method or by the penetration of a reference liquid.

The very nature of the structure in a paper strip would necessitate the determination of A by penetration studies. Efflux measurements utilizing either gases or liquids are impossible as the capillaries in the direction to be measured are parallel to the length of the paper. The capillary penetration of a reference liquid can be used to determine A if the contact angle between the paper and liquid is known.

Other investigators have shown that in general the contact angle depends upon the liquid used and the surface condition of the solid. The direct measurement of paper-liquid contact angles in paper capillaries obviously cannot be made. However, it should be possible to find a liquid whose rate of penetration would not vary with a change in the surface condition of the paper capillaries thus providing evidence of a zero contact angle in all instances. The conditioning of the surface must be accomplished by a method which will not alter the pore size by chemical or mechanical means and thus invalidate the results. McLean and Kohman[9] have shown that oxidation of paper does not affect the rate of penetration of benzene whereas it decreases the rate of penetration of water. This demonstrates that the paper-water contact angle has probably been changed; while that of benzene has remained unaltered, for oxidation would hardly be expected to change the structure of the paper, at least in such a way as to compensate exactly for a change in contact angle. Unpublished data have also shown the rate of penetration of benzene to be unaltered with other types of surface conditioning. A constant angle of contact with a changing surface condition would probably be equal to zero, but even if this were not the case, the assumption of a zero contact angle would still give results of practical importance. The constant error introduced in the A values for each paper strip by assuming a zero contact angle for the reference liquid when it is other than zero would alter the absolute values of the penetration constants of other liquids but not their relative values.

In view of these considerations, when a paper strip is calibrated with benzene and a second liquid is measured over the calibrated portion of the strip, the penetration constants relative to benzene can be determined by Eq. (4). It is obvious that the above equation cannot be expected to apply if the effective paths of flow are different for benzene and the second liquid. This condition may be brought about by swelling

[9] McLean and Kohman, Elect. Eng. **53**, 255 (1934).

of the fibrous structure or by mechanical dispersion of the loosely bound paper fibers. There seems to be no available information in the literature concerning the change in pore size of paper during impregnation with various liquids although Roth[10] has shown that the cell walls of pine wood increase in thickness with adsorption of water, i.e., the pore size diminishes. This has more recently been demonstrated by Stamm[11] who measured the flow of air at various relative humidities through wood sections. Since wood is a continuous structure and is therefore not subject to mechanical dispersion by liquid penetrants, each value of r in a general formulation must be replaced by $(r-\sigma r)$ where σ is the fractional decrease in the radius of each capillary brought about by swelling and would be equivalent to the internal swelling coefficient. It can be safely assumed that benzene does not swell pine appreciably, for Hasselblatt[12] found that benzene swells birchwood less than one percent externally, a figure which is believed to be approximately the same for internal swelling.

Paper, unlike wood, is a discontinuous structure of innumerable cellulosic fibers distributed in a more or less random manner and being rather loosely bound together. If these cellulosic fibers are assumed to be round incompressible rods, they might be arranged either in a closely packed incompressible condition or in a loosely packed compressible structure. The former would obviously result in increased pore size with swelling of the rods whereas the latter would more likely result in decreased pore size. It is believed that the loosely packed structure probably occurs in paper since pressure treatments followed by calendering are known to reduce the porosity of paper. It would appear from this that the effect of swelling liquids on paper would be similar to that on wood; but this is not necessarily the case, for mechanical dispersion of such a loosely bound structure may and probably does obtain during impregnation with liquids. The effects of mechanical dispersion may be larger than those of swelling in low density papers but may be less in more dense papers. Whether the pore size is increased or decreased depends therefore upon the type of paper and liquid used. It is also evident that with certain types of papers both effects might be alternately predominant which might cause fluctuations in the values of the penetration constants when check runs are attempted. Such fluctuations have been noted when dealing with water and other liquids which are known to swell cellulose but they are not reported here since the scope of the present investigation does not deal with the changes in pore size brought about by the penetration of liquids in paper strips. The possible effects of these have been considered merely to point out one of the inherent sources of error in the paper strip method.

[10] Roth, Bot. Ztg. **52**, 217 (1894).
[11] Stamm, Physics **6**, 334 (1935).
[12] Hasselblatt, Zeits. f. anorg. allgem. Chemie **154**, 375 (1926).

Experimental

The creosotes were held in an open dish in the original determinations by the paper strip method but it was found that, due to evaporation of volatile constituents, the viscosities had changed by as much as three percent after a single determination of 40°C. These results were disregarded and an apparatus designed which would remain closed throughout the course of a determination. This apparatus is shown in Fig. 1 with a paper strip in position for a penetration study. The paper is fastened to hooks on a glass rod by means of paper clips soldered to wire eyelets. A spring is added at the upper end to facilitate mounting and to keep the strips under a slight tension. The glass rod is suspended by a thread from a glass windlass by means of which it can be raised or lowered. Guides arrest rotation of the mounting so that a lamp placed behind the apparatus will furnish a clear view of the liquid meniscus at all times. The system can be evacuated by applying suction to the venting stopcock. Constant moisture conditions are maintained within the system by placing humidity controls such as dehydrite or saturated sodium chloride solution in the side bulb. By means of this arrangement the paper strip can be brought in contact with the liquid to be measured and the measurements made without disturbing the established equilibrium. The apparatus thus assembled is held vertically in an oil bath controlled at the desired temperature

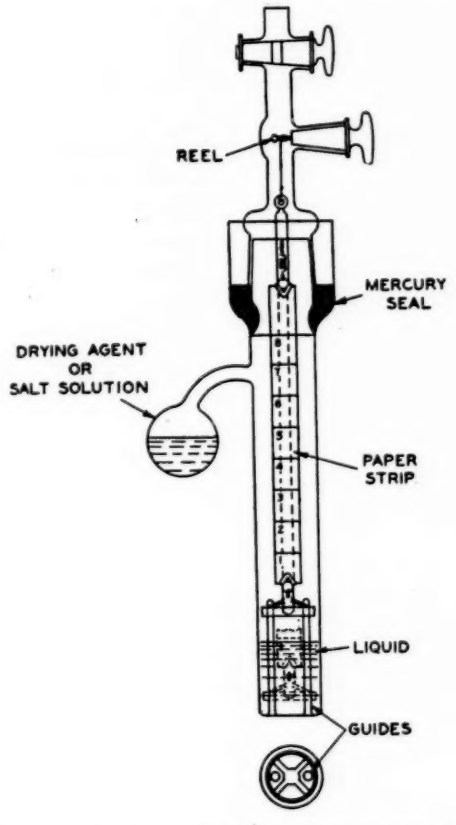

FIG. 1. Apparatus for studying penetration of liquids into paper strips.

with an accuracy of ±0.05°C by means of a mercury column thermostatic control.

In studying the rate of penetration into paper, strips approximately one cm wide are cut from a section of Whatman No. 4 filter paper. Each strip is lightly marked at half-cm intervals and successive markings are numbered. The strips are extracted with benzene to remove any extractives which might affect later results. Benzene is removed by drying at 60°C in vacuum and the samples are then conditioned in evacuated desiccators for at least one month. The humidities are controlled with dehydrite or saturated sodium chloride solution.

A sufficient quantity of benzene is placed in the apparatus with the side bulb containing one of the humidity controls. A paper strip is quickly transferred from the desiccator to the apparatus and slight suction is applied to prevent disruption of the mercury seal by the pressure developed with rise in temperature. The system is allowed to remain at constant temperature for at least 24 hours before the measurements are made. The paper is brought into contact with the benzene and the times of rise are taken at successive half-cm intervals. The paper is removed, dried at 60°C in vacuum and reconditioned in the original desiccator for another month. More than one determination with benzene was made on some of the papers to determine the reproducibility of the data.

The strips thus calibrated are used in the above manner to determine the times of rise of the Fulweiler creosotes at various temperatures. The data for benzene are all at 40°C but it is believed that the change in pore size due to expansion with increasing temperature is negligible. Whitehead and Greenfield[7] showed that pore size increased markedly with temperature increase but they do not mention any humidity control. Their relative humidity would be appreciably less at the higher temperatures and

TABLE I. *Some physical properties of the Fulweiler creosotes.*

Sample No.	Paper No.	Residue* Above 355°C (Percent)	Temp. (°C)	Viscosity (poises)	Surface Tension (dynes/cm)	Time of Rise** (Seconds) Benzene	Creosote
F-1	1	43.84	40	0.1064	38.35	174	2673
	2		60	0.0544	36.41	149(a)	1133
	3		80	0.0320	34.54	210	1036
	4		100	0.0218	33.66	194	615
F-2	5	40.25	40	0.0973	37.70	210	3008
F-3	6	31.11	40	0.0675	37.59	210	1917
	7		60	0.0377	35.63	193	1140
	8		80	0.0243	33.85	168(a)	670
	9		100	0.0170	32.24	190	526
F-4	10	28.52	40	0.0667	37.46	194	1897
F-5	11	20.85	40	0.0525	37.41	156	1184
	12		60	0.0310	35.57	196(a)	919
	13		80	0.0211	33.90	197	617
	14		100	0.0148	31.99	229(b)	560(b)
F-6	15	15.49	40	0.0445	37.49	194	1318
F-7	16	12.21	40	0.0396	37.52	191	1023
	17		60	0.0247	35.41	201	780
	18		80	0.0170	33.64	190	544
	19		100	0.0125	31.39	199	459
F-8	20	8.49	40	0.0344	37.01	190	968
	21		40	0.0344	37.01	199	953
	22		40	0.0344	37.01	184(c)	934(c)

* Standard distillation of creosote, Standard 11e, *American Wood-Preservers' Association Manual of Recommended Practice.*

** Time of rise between three and ten centimeters.

(a) Average of two or more benzene calibrations on the same paper strip.

(b) Average of two determinations on different paper strips.

(c) These determinations were made in equilibrium with saturated sodium chloride solution whereas the remaining ones were made in equilibrium with dehydrite.

consequently the amount of water adsorbed by the paper at the higher temperatures would be substantially reduced. The decrease in the amount of adsorbed water at the higher temperatures and consequent decrease in swelling might account for the large increase in pore size with increasing temperature which they found.

The added precaution is also taken, in measuring the rates of rise of the creosotes, to make the point of initial contact for the creosote coincide with that of the benzene calibration. This limits the penetration data for the creosotes to calibrated areas of the paper strips.

Paper strips were discarded after a single determination with any of the creosotes since long extraction of the papers with benzene still leaves the strips slightly discolored. This is probably due to large molecules insoluble in benzene and free carbon which are present in coal tar creosotes.

The penetration data thus determined are far too numerous for inclusion herein. The times of rise of benzene and the creosotes from 3 to 10 cm, as given in Table I, indicate the general trend of the data. The values of 3 and 10 cm are chosen as it is felt that initial inertia and final equilibrium effects are unimportant between these limits.

The surface tensions, viscosities and residues not distilling up to 355°C previously determined[1] for the Fulweiler creosotes are also included in Table I for reference purposes.

Repeated calibration of the paper strips with benzene gave successively lower values for the time of rise to the same height although this decrease in time was lessened by each successive determination. The explanation for this increased rate of penetration may lie in a general loosening of the cellulosic fibers as was previously discussed although it seems strange that the long extraction with benzene originally made on the papers did not eliminate this effect. The increased rates of penetration for benzene were not exceedingly large and only the average calibration values were included in Table I. The magnitude of these variations is clearly indicated in the slope values for benzene given in Table II.

It had been hoped that the effective radii of

TABLE II. *Penetration constants according to Eq. (4).*

Liquid	Temp. (°C)	Run No.	Slope (cm^2/sec.)	Intercept (cm/sec.)	$A\gamma \cos\theta$ (dynes)	$B \times 10^3$ (cm^2)
Benzene	40	1	0.399	−0.0155	0.00785	72.56
F-1	40	2	0.024	−0.0010	0.01021	79.78
Benzene	40	1	0.352	−0.0095	0.00693	44.47
Benzene	40	2	0.380	−0.0083	0.00748	38.85
Benzene	40	3	0.386	−0.0083	0.00760	38.85
F-1	60	4	0.046	−0.0010	0.01001	41.25
Benzene	40	1	0.337	−0.0161	0.00663	75.36
F-1	80	2	0.066	−0.0029	0.00845	71.38
Benzene	40	1	0.269	−0.0045	0.00529	21.06
F-1	100	2	0.080	−0.0012	0.00698	20.42
Benzene	40	1	0.270	−0.0045	0.00531	21.06
F-2	40	2	0.018	−0.0004	0.00701	29.29
Benzene	40	1	0.237	−0.0033	0.00466	15.45
F-3	40	2	0.025	−0.0003	0.00675	15.43
Benzene	40	1	0.264	−0.0040	0.00520	18.72
F-3	60	2	0.046	−0.0008	0.00694	23.29
Benzene	40	1	0.296	−0.0050	0.00583	23.41
Benzene	40	2	0.316	−0.0055	0.00622	25.75
F-3	80	3	0.075	−0.0011	0.00729	20.92
Benzene	40	1	0.275	−0.0051	0.00541	23.87
F-3	100	2	0.097	−0.0015	0.00660	20.25
Benzene	40	1	0.293	−0.0079	0.00577	36.98
F-4	40	2	0.030	−0.0007	0.00800	35.64
Benzene	40	1	0.329	−0.0061	0.00647	28.55
F-5	40	2	0.042	−0.0007	0.00882	28.18
Benzene	40	1	0.254	−0.0054	0.00500	25.28
Benzene	40	2	0.273	−0.0060	0.00537	28.09
Benzene	40	3	0.297	−0.0070	0.00584	32.77
F-5	60	4	0.058	−0.0012	0.00719	28.89
Benzene	40	1	0.254	−0.0028	0.00500	13.11
F-5	80	2	0.079	−0.0009	0.00667	14.98
Benzene	40	1	0.279	−0.0145	0.00549	67.87
F-5	100	2	0.101	−0.0028	0.00598	33.19
Benzene	40	1	0.274	−0.0045	0.00539	21.06
Benzene	40	2	0.285	−0.0048	0.00561	22.47
Benzene	40	3	0.290	−0.0045	0.00571	21.06
F-5	100	4	0.103	−0.0029	0.00610	34.37
Benzene	40	1	0.305	−0.0099	0.00600	46.34
F-6	40	2	0.047	−0.0017	0.00837	58.53
Benzene	40	1	0.276	−0.0056	0.00543	26.21
F-7	40	2	0.048	−0.0007	0.00760	21.53
Benzene	40	1	0.246	−0.0033	0.00484	15.45
F-7	60	2	0.066	−0.0010	0.00652	19.45
Benzene	40	1	0.286	−0.0064	0.00563	29.96
F-7	80	2	0.101	−0.0021	0.00687	28.56
Benzene	40	1	0.281	−0.0059	0.00553	27.62
F-7	100	2	0.117	−0.0023	0.00585	23.35
Benzene	40	1	0.243	−0.0024	0.00478	11.23
F-8	40	2	0.049	−0.0003	0.00674	8.09
Benzene	40	1	0.256	−0.0024	0.00504	11.23
F-8	40	2	0.051	−0.0005	0.00702	13.48
Benzene	40	1(a)	0.286	−0.0055	0.00563	25.75
F-8	40	2(a)	0.054	−0.0008	0.00743	21.56

(a) These determinations were made in equilibrium with saturated sodium chloride solution whereas the remaining ones were made in equilibrium with dehydrite.

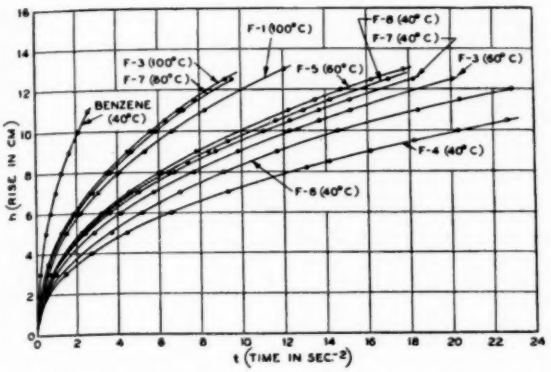

FIG. 2. Capillary rise of some of the Fulweiler creosotes in paper strips of approximately equal benzene calibrations.

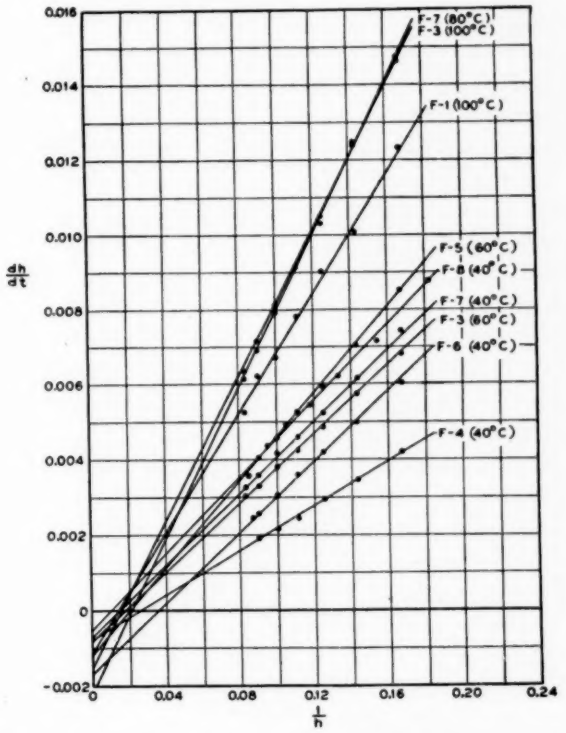

FIG. 3. dh/dt *vs.* $1/h$ for some of the Fulweiler creosotes in filter paper.

flow for the various papers might be quite similar since Whatman No. 4 filter paper was used throughout this work. The fallacy of such reasoning is immediately evident from the times of rise of the benzene calibrations as given in Table I. This has made it impracticable to compare the times of rise of the Fulweiler creosotes directly. However, it was possible to select several strips whose calibration values were quite similar (193 ± 3 seconds) for a height of rise extending from 3 to 10 cm. The corresponding height-time data for the penetration of the Fulweiler creosotes into these papers have been plotted in Fig. 2. These curves which should be directly comparable indicate that the rate of penetration in paper increases markedly with temperatures, the lower boiling creosotes are the better penetrants and the differences in the rates of penetration among the creosotes are less at the higher temperatures.

THEORETICAL RELATIONS

Theoretical and empirical considerations of experimental data offer a means of approaching the problems involved in the capillary penetration of fibrous materials with liquids. From a scientific viewpoint the applicability of established theoretical relationships to experimental data should always be considered before applying empirical relations. The latter should be used only to correlate data which do not conform to any of the known exact relations, to correlate data when there is no theoretical equation known or to establish a more simple correlation which would be more suited to the analysis of a great amount of experimental data. This portion of the discussion has therefore been limited to a consideration of the applicability of established equations of flow in capillaries based upon theoretical considerations as expressed by Eqs. (3) and (4).

It seemed more advisable, for reasons which become evident later in the discussion, to consider the applicability of the more complex Eq. (4) before Eq. (3). In so doing the method suggested by Peek and McLean[8] has been followed throughout and the values of dh/dt so obtained have been plotted against $1/h$ for some of the creosotes as shown in Fig. 3. The resulting straight lines are in good agreement with the theory developed by the above authors[8] and this agreement was found for all of the creosotes studied.

In Table II are listed the values of slope and intercept obtained with each of the creosotes tested, together with the values for their cor-

responding benzene calibrations. The corresponding values of $A\gamma \cos \theta$ (or 4η times the slope) and B (or $8\eta/dg$ times the intercept) have been computed according to Eq. (4) for each slope and intercept and these values are also included in Table II.

The benzene slope values listed in Table II indicate that Peek and McLean[8] must have been dealing with paper strips of very similar structure since they were able to use a single value of benzene slope for the calculation of the relative penetration tensions of the pure liquids which they investigated. The values of the benzene slopes given here vary by approximately 70 percent from the lowest value found. This stresses the importance of calibrating each strip of paper with a liquid such as benzene before determining relative values of any other liquid by this method.

The values of B (or $8\eta/dg$ times the intercept) shown in Table II are in reasonably good agreement for the same paper strip but they vary considerably among the different strips. The close agreement of the values of B determined with benzene and creosote show that this value is independent of the liquid used which is in accordance with the requirements of Eq. (4).

It is of interest to note that the values of $1/h$ when dh/dt is equal to zero afford a measure of the height to which a liquid will rise in a given paper strip providing the structure of the paper is assumed to be the same over this height as over the portion measured and that the theory can be assumed to extend to the ultimate height reached by the liquid. It is seen from the curves of Fig. 3 that the heights to which the creosotes for which data are plotted will rise vary from approximately 30 to 100 cm.

TABLE III. *Values of the ratio of the penetration tensions of the Fulweiler creosotes relative to benzene as determined in glass and paper.*

SAMPLE No.	40°C	60°C	80°C	100°C
F–1	1.12(1.04)	1.02(0.95)	1.04(1.00)	0.97(0.91)
F–2	1.09(1.04)	—	—	—
F–3	0.99(0.95)	1.02(1.05)	1.07(1.04)	1.01(0.98)
F–4	1.03(1.03)	—	—	—
F–5	1.04(1.01)	1.02(1.01)	0.97(0.94)	1.11(0.99)
F–6	1.02(1.08)	—	—	—
F–7	1.02(0.95)	1.00(1.05)	1.05(1.06)	1.13(1.09)
F–8	1.00(1.03)	—	—	—
F–8	1.01(0.97)	—	—	—
F–8(a)	1.07(1.02)	—	—	—

Note: The values of the above ratio which are shown in brackets were determined by Eq. (11) which will be discussed later. The remaining values were determined by Eq. (4).
(a) These determinations were made in equilibrium with saturated sodium chloride solution whereas the remaining ones were made in equilibrium with dehydrite.

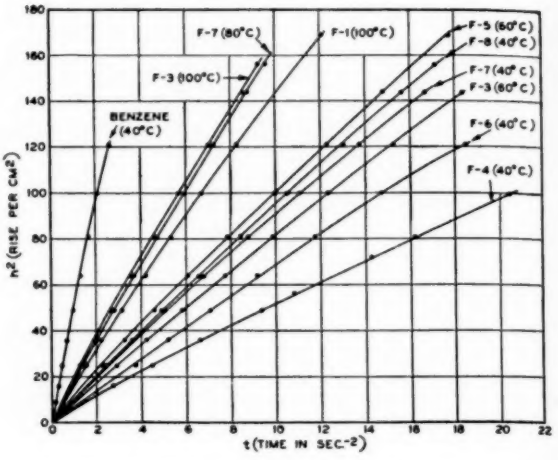

FIG. 4. Penetration of some of the Fulweiler creosotes into paper strips according to Washburn's equation.

The penetration tension values of the Fulweiler creosotes relative to benzene have been computed from the values of $A\gamma \cos \theta$ listed in Table II. The ratios of these values to the corresponding surface tension values relative to benzene are given in Table III. In the same table are also included values of the same ratio determined by an empirical equation but these need not be considered at present. The values of the ratio listed in Table II indicate that the ratio should be equal to one. The variations from unity are believed to be due to the limited accuracy of the paper strip method. This seems to be indicated by the lack of any definite check or trend when any one of the creosotes is considered at the various temperatures. It is concluded from this that the angles of contact for all of the Fulweiler creosotes are equal at all of the temperatures studied. As it would be very unlikely that all of the creosotes would have the same contact angle unless the latter were zero, it was also concluded that their angle of contact against paper is either zero or very small. This would also follow at once if the former assumption of a zero contact angle for benzene against paper is correct.

The plot of h^2 against t given in Fig. 4 shows that the data contained herein do not conform to the straight line relationship postulated by

Eq. (3). This slight but real curvature may have been caused by the small value of h when t was zero but it can be demonstrated that the possible error incurred in t would not account for the curvature found. Washburn obtained this equation by considering the hydrostatic head to be negligible when dealing with the capillary penetration of liquids into very small vertical capillaries. It has already been shown that the data contained herein conform to Eq. (4) which differs from Washburn's equation only in that the hydrostatic head and variations in pore size are considered. Since Eq. (4) integrates to give a form similar to (3) when hydrostatic head is neglected, it appears that the failure of Washburn's equation to fit the data must be due to neglect of hydrostatic effects. Whitehead and Greenfield[7] successfully applied Washburn's equation to their data probably because they considered only small heights of rise but it must follow that their values of r are somewhat in error because of neglect of hydrostatic head. Moreover, their values of r would not be those postulated by Washburn's equation but would be multiplied by the summation of some distribution function of r; i.e., their r would be the A of Eq. (4) except for the difference involved in not considering hydrostatic head.

While Eq. (4) is applicable to these data and is useful for fundamental research, it is somewhat difficult to apply in more practical problems where many data must be analyzed. It seemed advisable because of this to consider the applicability of empirical relations to the data in hand.

Empirical Relations

The logarithmic diagram for a few of the height-time data, as given in Fig. 5, is typical of all the experimental results. It is evident from these curves that the data obey the empirical relation of Bell and Cameron[2] as given by Eq. (1).* The values of n satisfying this equation were determined graphically and were found to vary from 2.00 to 2.38. These values for n are in good agreement with those found by Lucas.[4] Moreover, it was found that the values of n for the creosotes did not differ substantially from those of their corresponding benzene calibrations. Hence, it must follow that the differences in the values of n among the various paper strips used must have been caused by differences in the structural configuration of the paper strips.

Simmonds[5] has used the above equation for penetration studies but has assumed by analogy with Washburn's equation that $k=r\gamma/2\eta$. It can be shown from dimensional considerations that such an analogy is not justified.

The similarity of n for the penetration of creosote and benzene into the same paper strip shows that these liquids obey the same general laws in paper capillaries. It should therefore follow from Eq. (1) that

$$t(\text{benzene})/t(\text{creosote}) = C \qquad (7)$$

when the two liquids have been measured over the same area of a paper strip and the heights of rise are equal. The values of C should be constant for each creosote and temperature depending upon the physical properties of creosote in paper but should be independent of the original size, shape and distribution of the capillary pores in the paper. The values of C should therefore afford a simple and direct measure of the relative penetrability of the creosotes in paper providing variations among the paper strips are only of a structural nature. The latter seems reasonable when it is considered that all of the

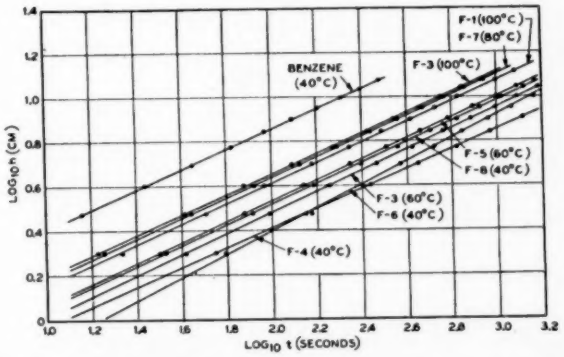

FIG. 5. Logarithmic h *vs.* t diagram for some of the Fulweiler creosotes in paper.

* The latter is based on the assumption that h is zero when t is zero which was not the case for these data although the equation was found applicable for the small values of h when t was zero. It was found impossible to remedy this condition because of the high initial speed of penetration especially in the case of benzene.

strips were not only prepared from the same lot of Whatman No. 4 filter paper but also received similar pretreatment.

It is also evident that any pore size changes brought about by either liquid would be correspondingly reproduced in C. The effects of benzene on the pore size should be relatively constant and need therefore not be considered, but the effects of creosotes on pore size may not be constant. The latter may be considered by some to give erroneous values of C but it is believed that this is not the case. In explanation, consider two creosotes which differ only in their ability to vary pore size. It is evident that the creosote maintaining the larger pore size during impregnation would penetrate the more rapidly and should therefore have the greater penetrating power. The values of C should therefore portray accurately any differences in penetrability among the Fulweiler creosotes since original structural differences among the paper strips have been eliminated by the benzene calibrations. The values of C have been computed and are listed in Table IV.

TABLE IV. *Penetrability of the Fulweiler creosotes relative to benzene as given by C.*

SAMPLE No.	40°C	60°C	80°C	100°C
F–1	0.0651	0.1316	0.2028	0.3155
F–2	0.0698	—	—	—
F–3	0.1095	0.1692	0.2506	0.3610
F–4	0.1022	—	—	—
F–5	0.1318	0.2132	0.3195	0.4082
F–6	0.1473	—	—	—
F–7	0.1866	0.2577	0.3497	0.4329
F–8	0.1965	—	—	—
F–8	0.2088	—	—	—
F–8	0.1969(a)	—	—	—

(a) These determinations were made in equilibrium with saturated radium chloride solution whereas the remaining ones were made in equilibrium with dehydrite.

The relative penetrabilities of the Fulweiler creosotes increase with volatility and temperature. A plot of the $\log_{10} C$ against the concentration of residue distilling above 355°C is shown in Fig. 6. The resulting curves are remarkable in that they show an inverse proportionality between $\log_{10} C$ at constant temperature and the volatility of these creosotes as expressed by

$$\log_{10} C = (E/c) + F \qquad (8)$$

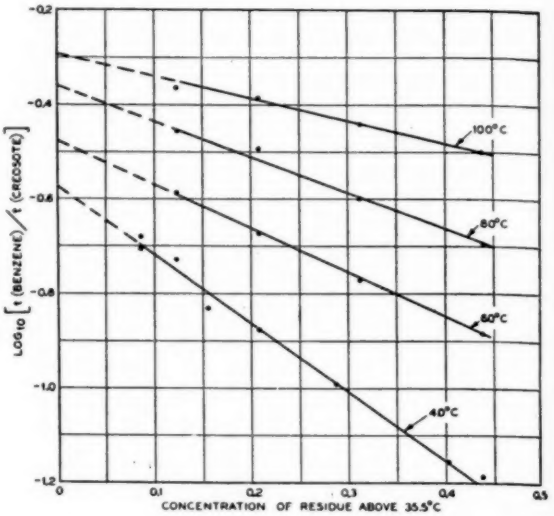

FIG. 6. Relative penetrability—concentration diagram for the penetration of the Fulweiler creosotes into paper.

where c is the concentration of residue not distilling up to 355°C and E, F are constants depending on the temperature. The effects of volatility upon the relative penetrability of the Fulweiler creosotes is demonstrated but the curves also show the desirability of using high impregnation temperatures with these creosotes. This is evident since the penetrability not only increases with temperature but the differences among the creosotes become less.

In another paper[1] it was shown that the $\log_{10}$ viscosity at constant temperature is directly proportional to the residue not distilling up to 355°C in these same creosotes. It should there-

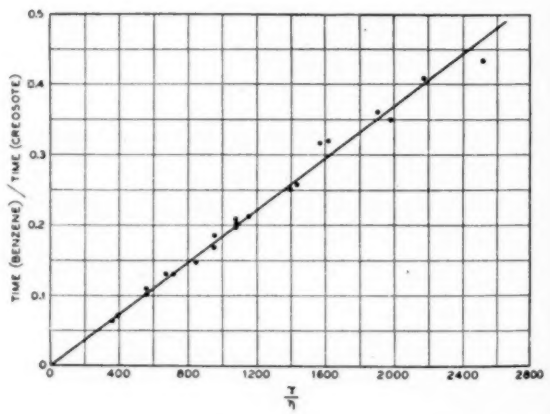

FIG. 7. C *vs.* γ/η for the penetration of the Fulweiler creosotes into paper strips.

TABLE V. *Values of* $G(C\eta/\gamma)\times 10^4$.

SAMPLE No.	40°C	60°C	80°C	100°C
F-1	1.806	1.966	1.879	2.043
F-2	1.801	—	—	—
F-3	1.966	1.790	1.799	1.904
F-4	1.820	—	—	—
F-5	1.850	1.858	1.989	1.889
F-6	1.748	—	—	—
F-7	1.969	1.798	1.767	1.724
F-8	1.826	—	—	—
F-8	1.941	—	—	—
F-8	1.830	—	—	—
Average	1.856	1.853	1.859	1.890

fore follow that the relative penetrability must depend upon some inverse function of the viscosity at constant temperature. Moreover, theoretical considerations of liquid flow in capillary systems would indicate that the relative penetrability should depend upon some direct function of the surface tension. In Fig. 7, C has been plotted against γ/η in accordance with the simplest relation suggested by the above reasoning. The points shown follow a straight line relationship remarkably well and indicate that

$$C=G\gamma/\eta \tag{9}$$

where G is a constant for all of the Fulweiler creosotes and is independent of temperature. The values of this constant are given in Table V.

The values of G taken as a whole vary quite considerably but it is suggested that it would be more suitable to consider average values in dealing with data which are known to be subject to fluctuating errors. When this is done the applicability of Eq. (9) to the data is demonstrated.

The relative penetrabilities of the Fulweiler creosotes have been shown to depend upon their respective viscosities and surface tensions in accordance with Eq. (9). It must follow accordingly that the times of rise of the Fulweiler creosotes into the same or identical paper strips should be directly proportional to their viscosities and inversely proportional to their surface tensions. Hence, since it has been shown that h^n is proportional to t when η/γ is held constant and t is proportional to η/γ when h is held constant, it must follow that

$$h^n=K\gamma t/\eta, \tag{10}$$

where n should be a constant for each liquid and paper depending upon the hydrostatic head as will be shown later and K should be a constant for each paper strip depending upon the structural configuration of the paper. It is evident from theoretical considerations that the dependence of K upon the structural configuration of the paper strips is based on the assumption of a zero or constant paper-liquid contact angle. Although this is apparently the case for the Fulweiler creosotes as was shown previously, it would evidently not always be true. Since the contact angle is known to reduce merely the effects of surface tension during penetration, the more general equation of flow may be written

$$h^n=K'\gamma\cos\theta t/\eta, \tag{11}$$

where K' would be dependent only upon the structural configuration of the paper.

An equation relating the factors affecting the penetration of the Fulweiler creosotes into paper strips has been derived from purely empirical considerations of experimental data. The ratios of the surface tensions of these creosotes determined in glass to the corresponding values of $\gamma\cos\theta$ determined in paper by the application of Eq. (11) are given in Table III. The values are in good agreement with those determined by Eq. (4) and the same conclusions of zero or small contact angle creosote-paper can be drawn from the results. It is also evident that the use of Eq. (11) for the determination of penetration constants is much the simpler of the two methods.

It will be noted that if Eq. (11) is considered in a differential form it will differ from Eq. (4) essentially in that no hydrostatic head term appears and that the h in the denominator of Eq. (4) has become h^{n-1} in the differential form of Eq. (11). It is concluded from this that the value of n empirically corrects Eq. (11) for the hydrostatic head term.

MOISTURE EFFECTS

The effects of different amounts of adsorbed water on the penetration constants of the Fulweiler creosotes were only considered at two moisture contents. It was felt that the close agreement in the values obtained did not war-

rant a complete investigation of the effects of water below fiber saturation. Moreover, unpublished data on other liquids have shown that varying amounts of adsorbed water do not change the values of the penetration constants. It must be remembered in this connection that any changes in pore size caused by the adsorbed water are eliminated from consideration since the height-time data for both the benzene calibration and creosote were determined on papers having the same moisture content.

It is believed that differences in the penetration constants of the Fulweiler creosotes might be found in the presence of free water for in this case interfacial tension effects would be introduced. The interfacial tensions of these creosotes have been shown[1] to vary greatly so that the contact angles between creosote and paper containing free water should also vary. The penetration tension ($\gamma \cos \theta$) would vary accordingly and consequently the rate of penetration into paper strips. The inclusion of a study of the rate of penetration into paper strips containing free water was not possible since methods for the duplication of conditions are not available. This is essential since the pore size of the capillaries must be taken into consideration by calibration with another liquid.

Heat Generation and Anisotropy of Rubber Compounds in the Flexometer

R. S. HAVENHILL, *Rubber Laboratory, St. Joseph Lead Company, Josephtown, Pennsylvania*
(Received March 28, 1936)

Data are given showing that it is possible for rubber to soften in one direction and stiffen in another direction simultaneously during a test in the St. Joe Flexometer. Both effects are mainly the result of heat, the softening being due to plastic flow, while the stiffening is due to the substantial elimination of plastic flow because of the rapidity of flexure. Static and dynamic tests on heated test pieces, and stress-strain data on various sections of test specimens at several stages of breakdown indicate that failure in dynamic tests is due partially to mechanical fatigue, but mainly to heat effects. Results on anisotropic pigments such as asbestine, clay, magnesium carbonate, and acicular and non-acicular zinc oxides show that the heat generation, breakdown time, flexing load, and vertical deflection are functions of the shape and orientation of the pigment particles. Variations in breakdown time from 16 to 160 minutes have been obtained by changing the orientation of pigment particles. Data on "grain" effect in high gum stocks are also given.

INTRODUCTION

IN a previous paper[1] a new machine for evaluating the breakdown characteristics of rubber compounds when flexed under compressive loads was described. This machine, which is known as the "St. Joe Flexometer," differs from previous flexometers in that the flexing forces can be measured at all times, and the end point is definitely indicated on the machine. With this machine it was shown that when rubber is flexed at a constant horizontal deflection under either constant vertical compression or constant vertical load an increase in flexing force is required to maintain the deflection at a constant value. No attempt was made in the previous paper to explain the phenomenon of the simultaneous occurrence of plastic flow and stiffening of rubber test specimens which was indicated by the data obtained. It was simply pointed out that the data showed good correlation with actual road tests on commercial solid tire and carcass stocks. While a general relationship between heat generation and breakdown time has been indicated[1, 2] a survey of the literature did not disclose any information regarding the phenomena taking place in rubber when flexed under compressive loads. In the present paper a study has been made of the simultaneous occurrence of plastic flow and stiffening action taking place, which has logically led to the investigation of anisotropy.

DESCRIPTION OF ST. JOE FLEXOMETER

Fig. 1 shows a view of the entire machine. Fig. 2 is a close-up view of the machine showing the sample under vertical compression and

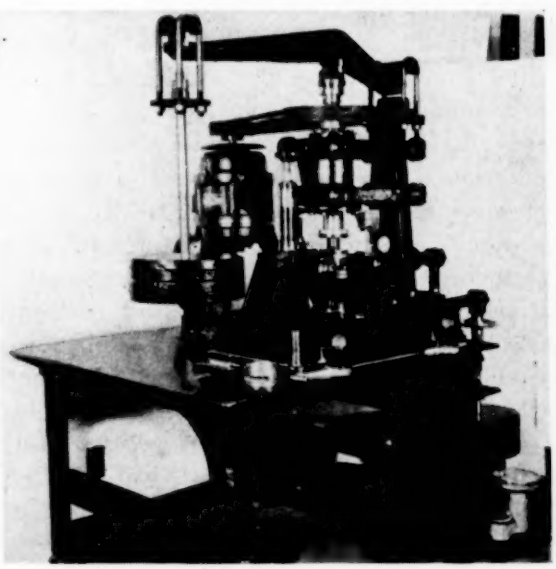

FIG. 1. View of the entire machine.

[1] Havenhill and MacBride, Ind. Eng. Chem., Anal. Ed. **7**, 60 (1935).
[2] Barnett and Mathews, Ind. Eng. Chem. **26**, 1292 (1934).

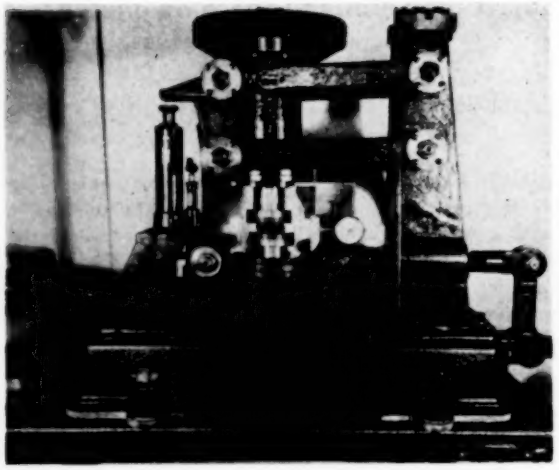

FIG. 2. Close-up showing a sample under vertical compression and horizontal deflection.

horizontal deflection. Fig. 3 is a drawing of the machine in which the various parts have been labeled.

The test specimen, which is a cylindrical plug 3.81 cm in diameter and 3.81 cm in height, is placed between the two parallel Bakelite face plates and under compression by means of the vertical load weight 6, acting through lever arm 7. The upper face plate is then rotated and the sample, which acts as a coupling, causes the lower plate to rotate. The lower face plate is mounted on the horizontal roller bearing carriage traveling on the track and can be moved off center from the upper plate any given amount by manipulation of handwheel 20. The load required to produce or maintain this horizontal deflection is read on scale 19. The horizontal deflection itself is read on dial 26. By a slight rotation of handwheel 20 the linkage 16 can be lengthened or shortened, thus decreasing or increasing the horizontal load and horizontal deflection on the sample. In this manner it is possible to run tests under constant horizontal deflection (*HD*) or under constant flexing load (*HL*). For a more complete description of the machine refer to the original article.

Fig. 4 shows what happens during a constant horizontal deflection test. The vertical load is maintained constant at 250 kg and the horizontal deflection is maintained constant at 0.673 cm. The horizontal load, vertical deflection or compression, and temperature at the center of the test specimen have been plotted against time. For these and subsequent tests, unless otherwise noted, the following formula was used:

	Parts by Weight
Rubber	100.0
Sulphur	4.0
D.O.T.G.	1.4
Gas Black	9.0
Zinc Oxide *	150.0

Cure 65 min. at 141.1°C

* Electrothermic process zinc oxide of medium particle size was used.
Average diameter[7] by number = 0.26 micron
Specific surface = 1.83 m^2/g

It will be noted that as the test progresses the vertical compression increases (height of test specimen decreases), which means that the sample is softening and flattening out. The horizontal load or flexing load, however, increases. This means that as the test progresses the force to produce a given deflection in the

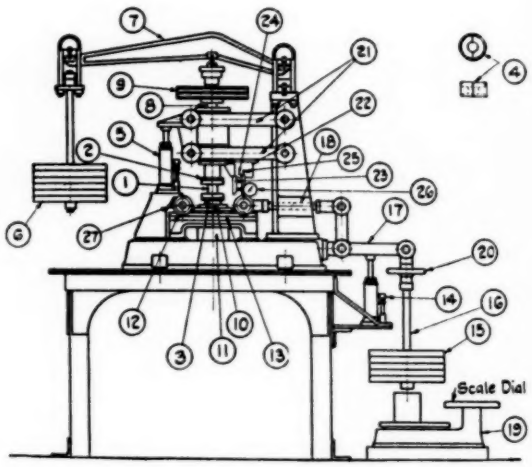

FIG. 3. Diagram of machine.

1. Rubber test specimen
2. Upper face plate
3. Lower face plate
4. Centering jig
5. Hydraulic jack
6. Vertical load weights
7. Lever
8. Upper vertical shaft
9. V-belt pulley
10. Lower vertical shaft
11. Carriage
12. Carriage rollers
13. Track
14. Hydraulic jack
15. Horizontal load weights
16. Hanger for weights
17. Bell crank
18. Link
19. Platform scale
20. Handwheel for deflection adjustment
21. Parallel linkage
22. Double divided scale
23. Straight edge for micrometer
24. Pointer for vertical compression
25. Pointer for horizontal deflection
26. Dial-type micrometer gauge
27. Carriage stop

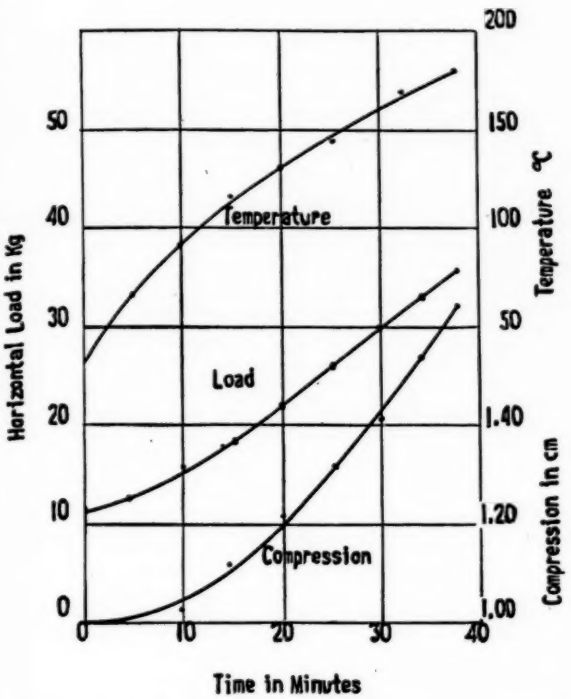

FIG. 4. Constant horizontal deflection test. Vertical load, 250 kg; horizontal deflection, 0.673 cm.

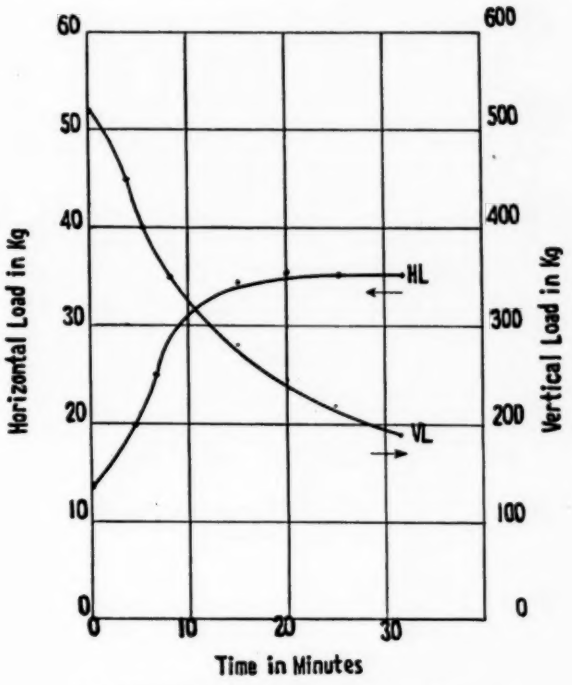

FIG. 4A. Constant vertical compression test. Vertical compression, 1.61 cm. Horizontal deflection, 0.714 cm.

horizontal plane increases, indicating a marked stiffening of the stock. The temperature also increases rapidly during the test, which is largely due to the combined effect of mechanical working and resultant frictional heat; the low heat conductivity and diffusivity of the rubber compound; and, in part, to the Joule effect.

Previous tests[1] carried out under constant vertical compression and constant horizontal deflection conditions show that the increase in horizontal load is not due to a change in the shape of the specimen, but is due primarily to a structural change or stiffening of the rubber. Evidence of this is presented in Fig. 4A.

SIMULTANEOUS STIFFENING AND PLASTIC FLOW OF RUBBER

To show how it is possible for the rubber to both soften and stiffen in different directions at the same time during a flexometer test, it was felt that if stress-strain data could be obtained for various sections of plugs run for different lengths of time in the flexometer, the data would throw some light on what was happening during test. The difficulties encountered in slicing, buffing, and dieing out tensile strips from the regular test specimens or plugs led to the use of a laminated plug. It was found that a specimen built up of disks (3.81 cm diameter and 0.19 cm in thickness) died out from vulcanized sheets would act as a unit in the flexometer, giving results which checked the results obtained by using the regular molded cylindrical plug.

Figs. 5, 6 and 7, show tensile strength, 100 percent modulus (stress at 100 percent elongation), and elongation at break data for laminated plugs run to 1/10, 1/2 and 9/10 breakdown in the flexometer. The tensile strength of the stock before flexing was 185 kg/cm^2; modulus at 100 percent elongation, 46 kg/cm^2; and elongation at break, 380 percent. The results show that during the first part of the test there is a slight increase in tensile strength toward the center of the plug. This is brought about by the cold working of the stock at relatively low temperature and is probably due to the formation of a new grain structure. As the test progresses the tensile strength gradually falls off due to the

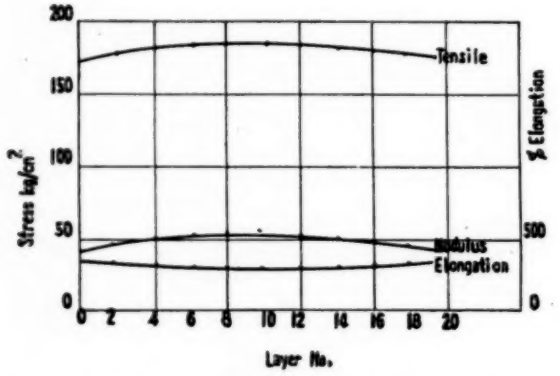

FIG. 5. Tensile strength at 1/10 breakdown time.

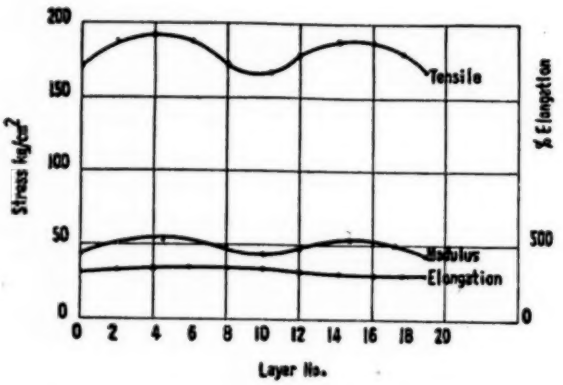

FIG. 6. Tensile strength at 1/2 breakdown time.

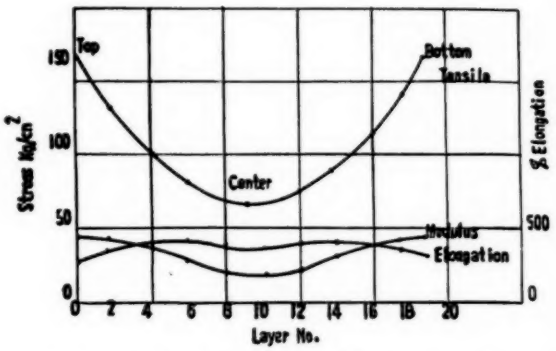

FIG. 7. Tensile strength at 9/10 breakdown time.

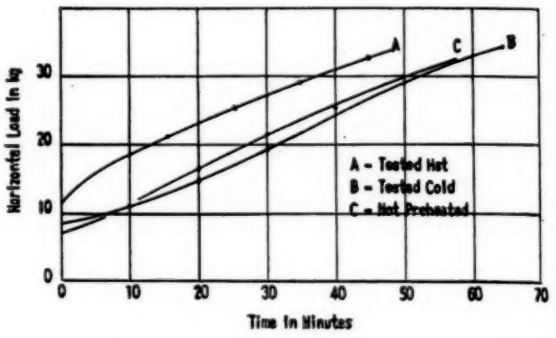

FIG. 8. Constant horizontal deflection tests on preheated specimens. Vertical load, 250 kg; horizontal deflection, 0.610 cm.

combined effect of heat, cure and mechanical working. These effects are greatest toward the center of the plug.

While these data show a slight increase in tensile strength during the first part of the flexometer test, they do not explain the increased stiffening of the specimens as the test progresses. Since the stiffness (as shown by the increase in horizontal load) is measured in the flexometer at high temperature, and the tensile strength was measured at low temperature, it was felt that the increased stiffening might be due to the effect of heat. In order to check this idea, plugs were heated for 20 minutes and then tested in the flexometer.

In Fig. 8 the horizontal load has been plotted against the time of test for samples preheated at 107°C, and tested while hot and after cooling. The curve for a specimen not preheated is included to show that the additional cure due to preheating causes a lower horizontal load. Similar curves for specimens preheated at other temperatures also indicate that the higher flexing load is a heat effect rather than a cure effect, and is a function of the temperature of preheating. In Fig. 9 the temperature of preheating has been plotted against the time of breakdown only, and it will be noted that as the temperature increases the breakdown time decreases. This relationship holds for tests in which the rate of heat generation is much greater than the rate of heat dissipation, as is usual test procedure in the flexometer. In the case of stocks (undercured stocks especially) tested under very low vertical loads and very low horizontal deflections so that the rate of heat generation approaches that of dissipation, this relationship may not hold true. These results indicate that the stiffening of the rubber is mainly a heat effect and that heat has a predominant influence on failure during flexing.

Since the heat generated by mechanical working and possibly the Joule effect has caused a stiffening in the horizontal plane, a similar stiffening effect might be expected in the vertical

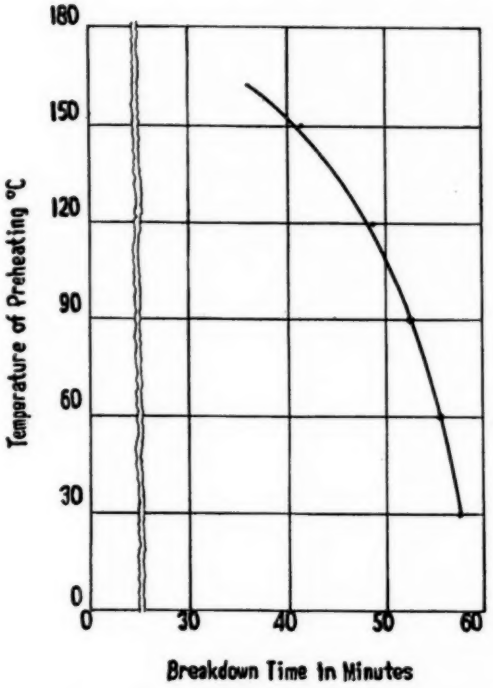

FIG. 9. Temperature preheating *vs.* breakdown time. Vertical load, 250 kg; horizontal deflection, 0.610 cm.

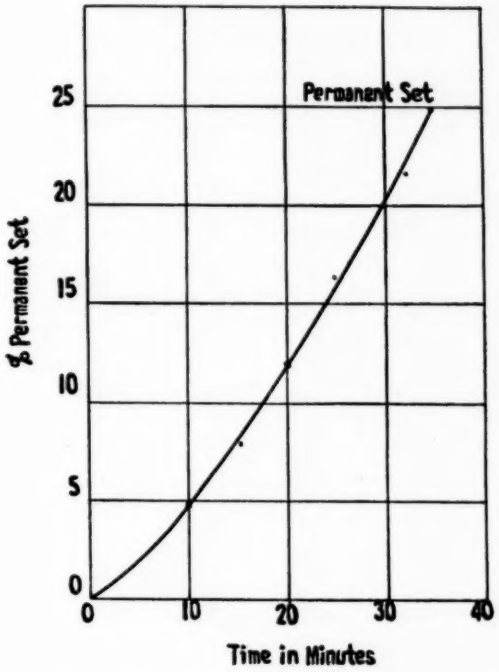

FIG. 11. Permanent set acquired during flexometer test. Vertical load, 250 kg; horizontal deflection, 0.673 cm.

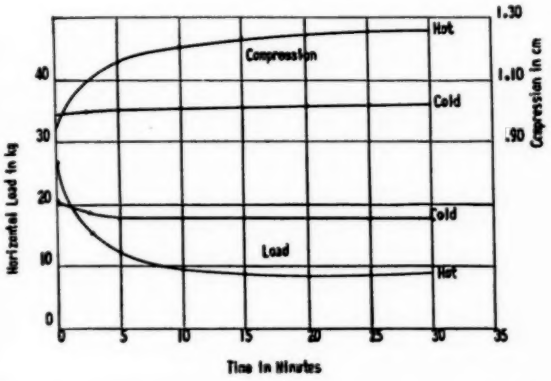

FIG. 10. Static compression test on hot and cold plugs. Vertical load, 250 kg; horizontal deflection, 0.714 cm.

plane. However, the results of flexometer tests show that during the test the samples actually soften and flatten out, and assume a permanent set. Static compression tests on heated plugs show that for the first ten seconds or so there is a slightly increased stiffness due to heat, but that plastic flow soon sets in and causes the flattening out and resultant permanent set.

Fig. 10 shows the data of such a static compression test run on a hot and cold plug. The first plug was heated 20 minutes at 157°C, cooled to room temperature, and then tested in the flexometer without rotation under 250-kg vertical load and 0.714-cm horizontal deflection. This plug showed slight evidence of plastic flow but there was no measurable permanent set at the end of 20 minutes. The other plug was heated 20 minutes and immediately placed in the flexometer under the same static conditions. The curves show that at the beginning of the test of the hot sample there is a stiffening in both the vertical and horizontal planes, as indicated by the initial high horizontal load and low vertical compression as compared with the cold sample. After the first few seconds of test plastic flow sets in as shown by the rapid increase in vertical compression (flattening out of the sample) and decrease in horizontal load. This plastic flow results in a permanent set. Fig. 11 shows permanent set data plotted against time of test. These data were obtained by stopping several dynamic tests at different stages of breakdown. Since it was found that the set measured after a 24-hour rest period was very nearly the same as that measured on the hot

plugs immediately after the test, only the set after 24 hours is shown. In the dynamic or regular flexometer test the specimen is flexed so rapidly in the horizontal plane (875 r.p.m.) that plastic flow in that plane cannot take place to any substantial degree. In the vertical plane the compressive force acts continuously in the same direction, so that flow does take place. This rapid flexing and reversal of stress in the horizontal plane without flexing in the vertical plane makes it possible for the particular rubber compounds tested to exhibit the simultaneous stiffening and plastic flow during the flexometer test.

These data show very definitely that rubber is stiffer at high temperatures than at low temperature when plastic flow is substantially eliminated. From thermodynamic considerations also[3, 4] we would expect the rubber to be stiffer at increased temperatures. While ordinary stress-strain data[5] usually show a lower modulus at high temperatures, stress-strain tests made at very high speeds[6] show a higher modulus for temperatures up to 140°C. Higher modulus could undoubtedly have been obtained on the layers of laminated plugs (Figs. 5, 6 and 7) if the stress-strain tests had been made at a higher speed than is customary with the standard stress-strain machine, and at the temperatures reached in the flexometer test.

Anisotropy

Since rubber compounds when tested in the flexometer exhibit simultaneous plastic flow and stiffening in different directions, it might be expected that pigments having different particle shapes would, when incorporated into the rubber stocks, produce anisotropy of the compounds and exert a pronounced effect on heat generation. Since no mention is made in the literature regarding the effect of anisotropy on heat generation, the following data are presented.

It was first thought that tests could be made on cubes built up from layers each having the grain in one direction. These cubes could then be tested with any one of the three axes in the vertical plane of the machine to show the differences in breakdown characteristics due to "grain" effects and orientation of the pigments.

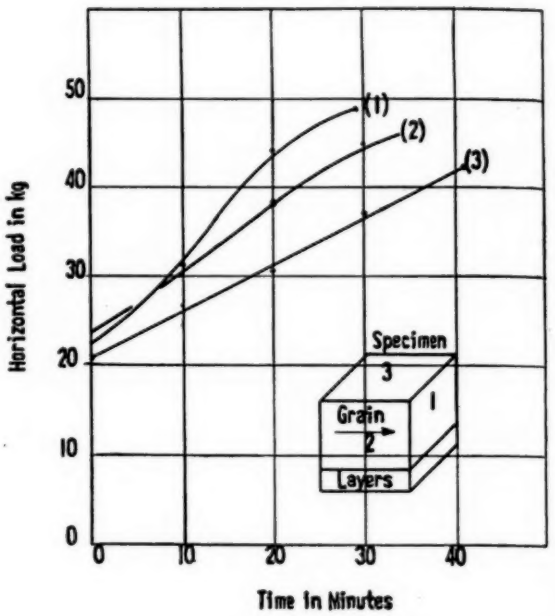

FIG. 12. Test on cubic plug. Vertical load, 290 kg; horizontal deflection, 0.760 cm.

It might be mentioned here that the resistance to shear of a block of wood along the grain is less than that across the grain, and much less than that perpendicular to the grain. The horizontal load might be considered analogous to the shearing force, and the facing of the test piece in the flexometer would determine whether shear should occur with, across, or perpendicular to the "grain."

Fig. 12 shows results of tests on a 3.81 cm cube of the same stock as that used for tests shown in Fig. 4. Numbers at the end of the curves indicate the top face of the specimen during test. Because of unequal stresses in the different directions, considerable vibration was encountered and duplicate results were very hard to obtain. The cubic test specimen was then discarded and the molded cylindrical specimen was used. To align the pigment particles in different directions, three methods of preparing the samples prior to vulcanization were used. *Method 1:* The uncured stock is sheeted out after remilling for two

[3] Gerke, Ind. Eng. Chem. **22**, 73 (1930).
[4] Wiegand and Snyder, Rubber Chem. Tech. **8**, 151 (1935).
[5] Somerville and Cope, India Rubber World **79**, 64 (1928).
[6] Williams, Ind. Eng. Chem. **21**, 872 (1929).

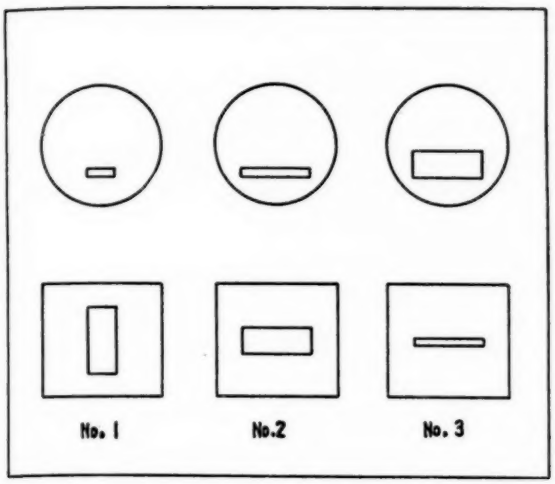

FIG. 13. Pictorial representation of the orientation of a rectangular plate-shaped pigment particle.

minutes on a laboratory mill (roll temperature 49°C) to 0.381 cm thickness. After a 2-hour rest period, strips 5.08 cm wide, with a length equal to the width of the sheeted stock are cut off across the grain and rolled up, making the grain of the rubber parallel to the axis of the cylinder. *Method 2:* In this method strips are cut in the direction of the grain of the sheeted stock and rolled into cylinders. Here the pigment particles are in a spiral perpendicular to the axis of the specimen. *Method 3:* In this method disks died out of the uncured stock are built into a laminated specimen having the pigment particles in layers perpendicular to the axis.

Fig. 13 is an exaggerated pictorial representation of the orientation of a rectangular plate-shaped pigment particle subjected to the three methods of preparing samples.

Microscopic examination showed that pigment particles were lined up during milling with their longest dimension in the direction of milling and their shortest dimension normal to the rolls. Examination of the stocks to be tested showed that this alignment was present after vulcanization. If we consider a pigment having needle- or rod-shaped particles, these particles would be aligned, in method 1, with the long dimension parallel to the axis of the cylinder. In the flexometer the needles would be vertical, and would offer greatest resistance to the horizontal load or flexing force. During the constant horizontal deflection test, we would expect a high horizontal load and a relatively short breakdown time due to the rapid heat generation. In methods 2 and 3 the small dimension of the particles would be parallel to the axis of the test specimen, offering a low resistance to the horizontal load or flexing force, and we would consequently expect lower flexing loads and longer running time in the flexometer test.

If we consider plate-shaped particles with square or round faces, we would expect high flexing loads with short breakdown times in methods 1 and 2 where the larger dimension of the particle is parallel to the vertical axis, offering greater resistance to the flexing load. In method 3 the plates would form a laminated structure in which the thickness of the particle would be parallel to the vertical axis, and we would expect a much lower horizontal load and much longer breakdown time.

If the pigment particles are rectangular plates, we would expect method 2 to give a lower flexing load and longer breakdown time than method 1. Method 3 would give much lower

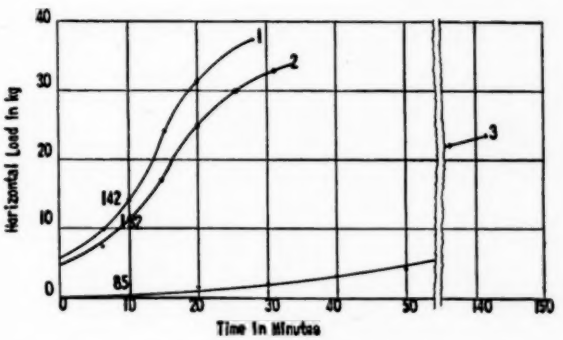

FIG. 14. Constant deflection tests on stock containing clay. Vertical load, 250 kg; horizontal deflection, 0.570 cm. Curves 1, 2 and 3 indicate method of preparation.

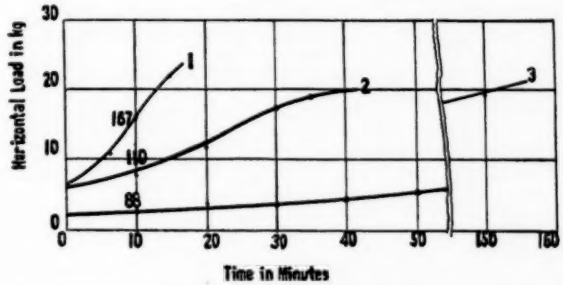

FIG. 15. Constant deflection tests on stock containing asbestine. Vertical load, 250 kg; horizontal deflection, 0.661 cm. Curves 1, 2 and 3 indicate method of preparation.

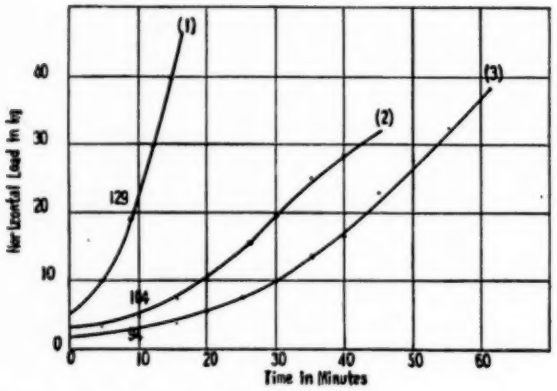

FIG. 16. Constant deflection tests on stock containing acicular ZnO. Vertical load, 250 kg; horizontal deflection, 0.635 cm. Curves 1, 2 and 3 indicate method of preparation.

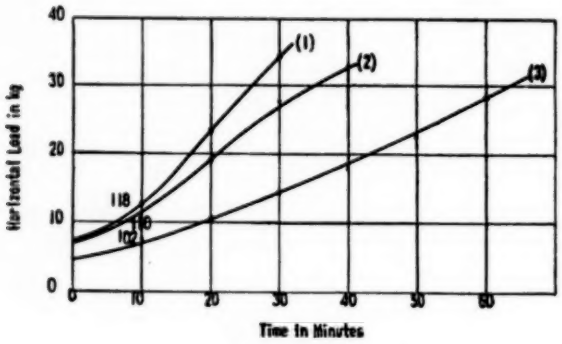

FIG. 17. Constant deflection tests on stock containing nonacicular ZnO. Vertical load, 250 kg; horizontal deflection, 0.661 cm. Curves 1, 2 and 3 indicate method of preparation.

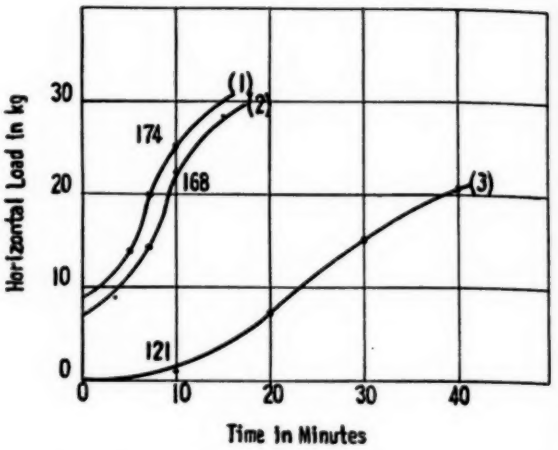

FIG. 18. Constant deflection tests of stock containing magnesium carbonate. Vertical load, 250 kg; horizontal deflection, 0.508 cm. Curves 1, 2 and 3 indicate method of preparation.

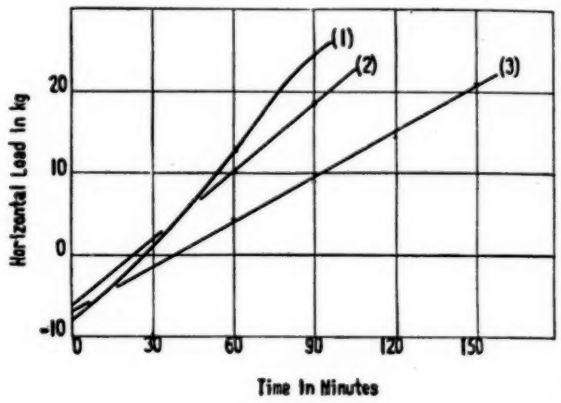

FIG. 19. Constant deflection tests on pure gum stock. Vertical load, 215 kg; horizontal deflection, 1.130 cm. Curves 1, 2 and 3 indicate method of preparation.

flexing load and considerably longer running time than method 2.

In order to check this theory, stocks were made up by using the formula referred to above with all but one volume of zinc oxide replaced by equivalent volume loadings of magnesium carbonate, clay, asbestine, acicular zinc oxide and nonacicular zinc oxide. These stocks were tested in the flexometer with a constant vertical load of 250 kg and constant horizontal deflections indicated on the graphs.

Figs. 14, 15, 16, 17 and 18 show the horizontal load-time curves obtained in the tests. The temperature at the center of the test specimen after 10 minutes of flexing is indicated along the curves. The method of preparation of the plug, which indicates the grain direction, is given by the number at the end of each curve. A high-gum stock (the above formula without pigment) is shown in Fig. 19 for the purpose of comparison. Temperature measurements were not taken during tests of this stock in order to eliminate any possible tendency of the hypodermic-needle thermocouple to cause premature failure. Samples of high-gum stocks generally have a tendency toward a mechanical type of failure. Table I includes time, vertical compression, horizontal load, and temperature data for each test at the start, after 10 minutes, and at the breakdown point.

Results of the flexometer tests on stocks containing clay (Fig. 14) show that the breakdown characteristics of test specimens prepared by methods 1 and 2 are very similar, while in those prepared by method 3 the horizontal load

is lower and the running time considerably longer, with slow heat generation. These data indicate that the particles are thin plates.

In the case of stocks containing asbestine (Fig. 15) the differences in breakdown characteristics between specimens prepared by methods 1 and 2 are very pronounced. This indicates that the length of the particle is considerably greater than the width. The very low flexing load, long time, and slow heat generation of specimens made by method 3 indicate that the thickness of the particle is considerably less than either the length or width. In effect, the particles of asbestine act as if they were long thin needle-like crystals or ribbons.

The curves for stocks containing acicular zinc oxide (Fig. 16; the oxide used being an American process product having an average diameter[7] of 0.36 micron and a specific surface of 1.54 m^2/g) show that specimens made by method 2 run for a much longer time under a lower flexing load than specimens made by method 1. These data indicate that the length of the particle is much greater than the width, and the similarity of the curves for specimens made by methods 2 and 3 show that the thickness is about the same as the width, indicating a close approach to the true needle shape.

For nonacicular zinc oxide (Fig. 17) the data indicate a more nearly isotropic shape.

The results of these tests enable the prediction of particle shapes which check fairly closely those shown by microscopic examinations of the pigments used. However, breakdown characteristics of plugs made by method 3 show greater

[7] Perrott and Kinney, J. Am. Ceramic Soc. **6**, 417 (1923).

TABLE I. *Test of stock with various pigments.* VC = vertical compression. HL = horizontal load. Values are given at starting time, at the end of 10 minutes and at the time of breakdown.

Pigment	Period of Test	Method of Preparation	Time (min.)	VC (cm)	HL (kg)	Temp. (°C)
Clay $HD = 0.570$ cm	Start	1	0	1.16	7.0	30
		2	0	1.14	5.5	30
		3	0	1.19	0.0	30
	10-min.	1	10.0	1.38	14.8	142
		2	10.0	1.32	11.5	132
		3	10.0	1.23	1.0	85
	Break	1	27.5	2.14	38.0	216
		2	34.5	2.12	35.0	213
		3	141.0	2.03	23.0	205
Asbestine $HD = 0.661$ cm	Start	1	0	1.08	7.0	30
		2	0	1.04	6.0	30
		3	0	1.08	3.0	30
	10-min.	1	10.0	1.35	15.0	168
		2	10.0	1.05	8.0	110
		3	10.0	1.10	3.0	88
	Break	1	17.0	1.75	24.0	213
		2	41.0	1.82	20.0	218
		3	157.5	1.85	22.0	196
Acicular Zinc Oxide $HD = 0.635$ cm	Start	1	0	1.14	5.5	30
		2	0	1.04	3.4	30
		3	0	1.12	2.0	30
	10-min.	1	10.0	1.50	21.8	129
		2	10.0	1.14	5.5	104
		3	10.0	1.17	3.4	94
	Break	1	16.5	1.93	46.3	200
		2	45.3	1.90	32.0	198
		3	61.5	1.98	38.2	182
Nonacicular Zinc Oxide $HD = 0.661$ cm	Start	1	0	1.16	8.0	30
		2	0	1.02	7.5	30
		3	0	1.09	5.0	30
	10-min.	1	10.0	1.13	12.7	118
		2	10.0	1.04	12.2	110
		3	10.0	1.14	7.8	102
	Break	1	32.0	1.70	36.0	177
		2	41.0	1.62	33.0	176
		3	66.5	1.70	31.5	175
Magnesium Carbonate $HD = 0.508$ cm	Start	1	0	1.40	9.0	30
		2	0	1.35	7.0	30
		3	0	1.32	0.0	30
	10-min.	1	10.0	1.94	25.1	174
		2	10.0	1.86	21.8	168
		3	10.0	1.52	1.0	121
	Break	1	16.0	2.24	30.5	208
		2	16.5	2.21	29.5	207
		3	40.0	2.20	21.2	192
High Gum $HD = 1.130$ cm	Start	1	0	1.75	−8.0	30
		2	0	1.71	−6.5	30
		3	0	1.68	−7.0	30
	10-min.	1	10.0	1.68	−5.7	—
		2	10.0	1.65	−4.0	—
		3	10.0	1.63	−4.5	—
	Break	1	96.0	1.98	26.5	—
		2	106.5	1.90	23.5	—
		3	159.0	1.90	23.0	—

differences from characteristics of methods 1 and 2 than would be predicted by the theory and microscopic studies. These differences would indicate anisotropy of the rubber hydrocarbon itself, and the curves for the high-gum stock (Fig. 19) show evidence of such anisotropy which may possibly vary in its effect with different pigments in compounded stocks. This long running time of specimens prepared by method 3 is also in part due to the fact that the stock is approaching the point at which heat dissipation is as rapid as heat generation.

As a further check on the theory, flexometer tests were run on a stock containing magnesium carbonate. From the curves of Fig. 18, a thin plate-shaped particle was predicted. This shape differs from the usual one which is needle-like, but a microscopic examination revealed that the plate type of particle was actually predominant.

While the data in general check the theory, which is based on particle shape, there is evidence of other factors which enter into the picture so that quantitative predictions cannot be made. Several of these factors are "skin" effect in the laminated plugs, possible lack of complete alignment of particles in the milling operation, and variable anisotropy of the rubber itself in different compounds. There is also microscopic evidence of a breaking up of some of the pigment particles during test.

Conclusions

Data have been presented to show that it is possible for rubber compounds when tested in the flexometer to exhibit simultaneously a plastic flow in one direction, and a marked stiffening in another direction resulting from the elimination of plastic flow by rapid flexing. Both effects are shown to be due mainly to heat generation or temperature effects. The rate of heat generation is in part dependent on the anisotropy of the rubber compound, which is much greater than is indicated by some of the ordinary physical tests such as tensile, tear and abrasion. The theory that the degree of anisotropy is influenced by the shape and orientation of the pigment particles and of the anisotropy of the rubber itself has been in a measure experimentally verified.

The Effect of Pigment Particle Size on Some Physical Properties of Rubber Compounds

C. E. BARNETT,* *New Jersey Zinc Company*

(Received March 28, 1936)

The stresses around large obstacles in strained rubber were studied with the assumption that the effects would be similar with actual pigment particles. The effects of variations in the size and shape of the obstacles on the stress concentration were investigated and an explanation offered for the stiffening of rubber by pigments based on the change in slope of the rubber stress strain curve. The various average diameters of a series of zinc oxide samples were measured and their relationship with some physical properties of rubber compounds determined.

THE importance of flow in the rubber on the reinforcing properties of pigmented systems has been emphasized by Park.[1] He suggests: (1) that in the presence of a finely divided pigment, the flow which occurs when a piece of rubber is stretched, takes place in the capillary spaces between the pigment particles; (2) that some modification of the laws of liquid flow may govern the behavior of rubber with reference to pigments embedded in it; and (3) that the forces causing increased stiffness in pigmented rubber compounds are similar to those causing increased resistance to flow of liquids in tubes of capillary dimensions. Thus increasing fineness of subdivision and the resulting fineness of capillary spaces between the particles should be accompanied by an increase in reinforcing properties.

It would be desirable to study the actual stresses around pigment particles in rubber under strain but so far no suitable microscopic set-up has been devised. A few years ago the writer, resorting to analogies, measured the strains and stresses around large particles with the assumption that the strains would be relatively the same with small particles. For this study holes of the desired size and shape were cut in strips of calendered but uncured gum stock and fitted with pieces of an uncured semihard rubber compound. After vulcanization squares were marked on the tensile sheets as shown in Fig. 1.

With no particles in the sheet the strains remained uniform on elongation as shown by Fig. 2. However, when particles were inserted, as in Figs. 3 to 7, the stresses became uneven and strains were greater around the particles. These uneven strains caused by the particles resemble very much the lines of flow of a liquid past an object. The percentage elongation was obtained from the photographs and, with the load known, it was possible to draw the stress strain curve for any part of the tensile sheet.

In Fig. 8, stress is shown for varying distances from the particle for circular and rectangular particles. When no particle is present the corresponding stress in the rubber is 125 pounds per square inch, corresponding to 225 percent elongation, and this stress is shown by the horizontal line. All of the curves approach this line as the distance from the particle increases.

Two conclusions are possible from Fig. 8.

1. Stresses are greater at the surface of large particles than smaller ones. This checks Schippel[2] who found that for the same material the volume increase under strain varied directly with the particle size.

2. The stress in the vicinity of a rectangular particle is great if the particle is oriented with its length parallel to the direction of pull but small if oriented normal to this direction.

The stress strain curve of unpigmented rubber may be considered as of two parts, one parallel to the strain axis (soft) and the other parallel to the stress axis (stiff). According to Figs. 3 to 8, the addition of pigment causes the strain on considerable of the rubber to be raised to the stiff part of the stress strain curve when the average rubber would normally be in the soft part of the curve.

The magnitude of this stiffening action may be determined by the size, shape, size distribution or dispersion of the pigment. Fig. 9 shows a series

* Investigator, Research Division, The New Jersey Zinc Company, Palmerton, Pa.

[1] C. R. Park, News Ed., Ind. Eng. Chem. **11**, 345 (1933).

[2] Schippel, Ind. Eng. Chem. **12**, 33 (1920).

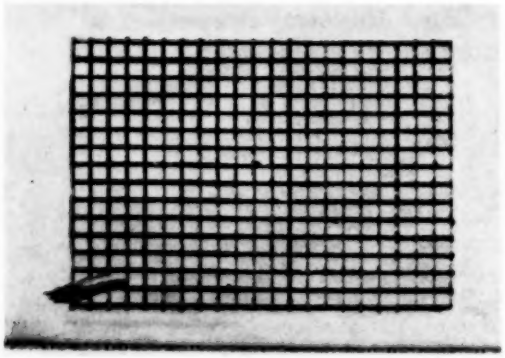

FIG. 1. Marking of vulcanized squares.

of stress strain curves for circular and rectangular particles. The values for the stress are those found by extrapolating curves similar to those in Fig. 8 to the stress axis. The elongations, as abscissae, are those for the rubber as a whole. Here again the greatest stiffening is obtained with the rectangular particle oriented lengthwise to the direction of extension. In the case of the circular particles, the magnitude of the stiffening by the particle depends on its diameter. Between particles of one and two centimeters in diameter, there is an increase in strain of 32 percent for the section of maximum concentration of stress; between particles of one and three centimeters in diameter, the increase is 48 percent. These increases are in the ratio of one to one and one-half which is the same as the ratio of diameters. It has been calculated[3] that for an expanded tetrahedral arrangement (which gives a greater interparticulate distance than an expanded cubical arrangement) in a 20-volume carbon black stock the particles are distant from each other slightly more than their own radius. Yet Figs. 3 to 7 have shown that the field of influence of the particles extends well beyond the distance represented by the radius of the particles; thus these effects would tend to be relatively greater in a rubber compound containing a moderate amount of pigment.

From the information accumulated in work with actual pigments in rubber, two general theories have developed. The one based on abrasion, tear and stress-strain studies assumes a heterogeneous structure to be responsible for

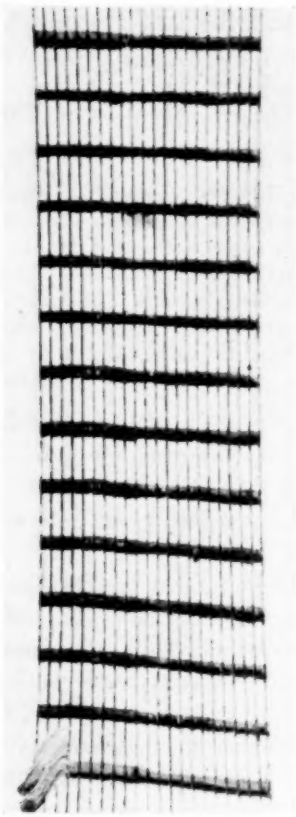

FIG. 2. Uniform strain, no particles in the sheet.

reinforcement by increasing stiffness. An attempt to give the mechanism of this action has been made in this paper. The second based largely on stress strain measurements and heat of swelling data explains reinforcement as a surface phenomenon. Among those attacking the problem from the first angle Haslam[4] has endeavored to determine which of the various average diameters of a pigment was most significant in determining the physical properties of rubber and how great an error would result if an average diameter other than the correct one were used. Mixtures of four zinc oxide samples of different particle size were prepared so that several samples had the same surface area but differed in number of particles per unit weight while others differed in surface area but had the same number of particles per unit weight. Stress strain properties, abrasion and tear resistance were measured on the rubber

[3] Wiegand, India Rubber J. **73**, 31 (1927).

[4] Haslam, The Rubber Age (N. Y.), Nov. 10, 1932.

FIG. 3.

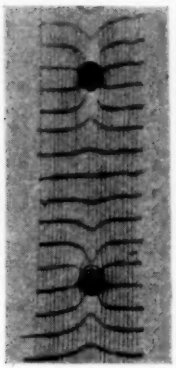

FIG. 4.

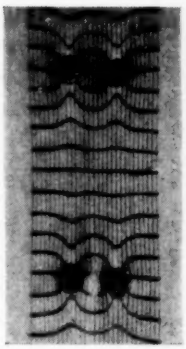

FIG. 5.

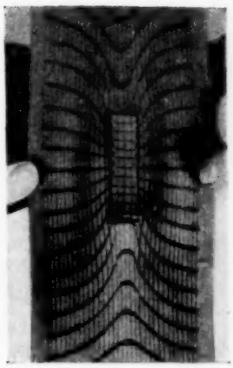

FIG. 6.

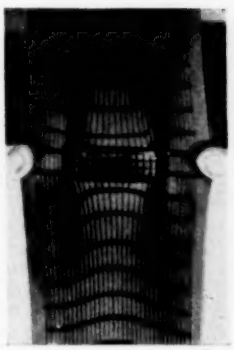

FIG. 7.

FIGS. 3 to 7. Nonuniform strains produced by the insertion of particles.

compounds. In general, as the specific surface or the number of particles were increased the reinforcing properties improved with the better relationship in the case of specific surface. However, even in the samples in which specific surface was held constant, the physical properties varied somewhat and these variations were ascribed to variations in uniformity since they were proportional to the variations between the particle sizes of the component oxides. Table I gives the various diameters, the specific surface, number of particles per gram and uniformity coefficients of a series of pigments and pigment mixtures prepared according to the method of Haslam as well as the equations used in their calculation. A lengthy discussion of these diameters is not justified here since the subject has been covered by Perrot and Kinney[5] and by Green.[6] d_1 is the arithmetic mean diameter, d_3 the diameter from which specific surface may be calculated, D the diameter from which the number of particles per

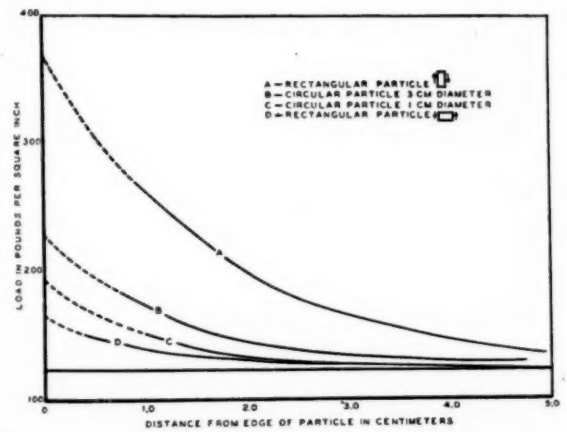
A—RECTANGULAR PARTICLE
B—CIRCULAR PARTICLE 3 CM DIAMETER
C—CIRCULAR PARTICLE 1 CM DIAMETER
D—RECTANGULAR PARTICLE
LOAD IN POUNDS PER SQUARE INCH
DISTANCE FROM EDGE OF PARTICLE IN CENTIMETERS

FIG. 8. Stress in pounds per square inch *vs.* distance from edge of particle.

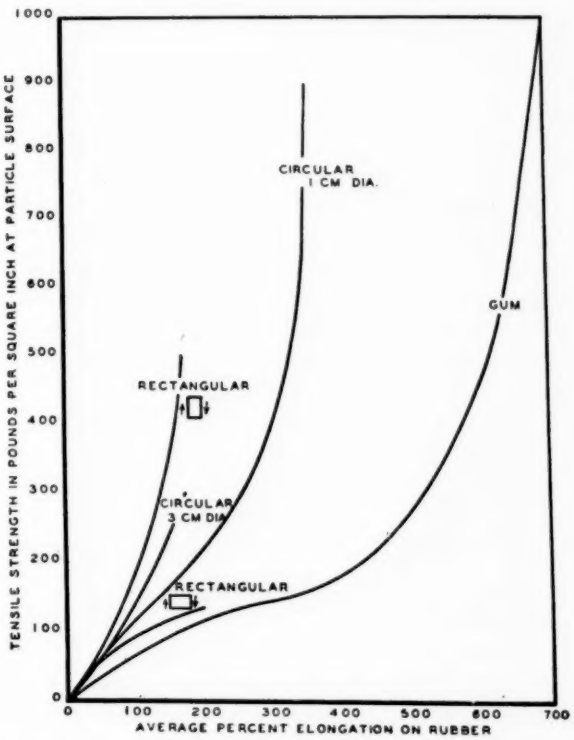

FIG. 9. Stress *vs.* strain for various shapes of particles.

[5] Perrot and Kinney, J. Am. Ceramic Soc. **6**, 417 (1923).
[6] Green, J. Frank. Inst. **204**, 713 (1927).

TABLE I. *Various diameters, the specific surface, number of particles per gram and uniformity coefficients of a series of pigments and pigment mixtures.* Equations defining these quantities in terms of the density (ρ), the number of particles of various sizes (n), and the fraction weights of components of mixtures (w).

$$S=\frac{6}{\rho d_3},\quad N=\frac{1}{\rho D^3},\quad d_1=\frac{\Sigma nd}{\Sigma n},\quad Ud_1=\frac{\Sigma d_1 w}{\Sigma w},\quad \Delta=\left(\frac{\Sigma nd^2}{\Sigma n}\right)^{\frac{1}{2}},\quad U=\left(\frac{\Sigma w/d^2}{\Sigma w/D^2}\right)^{\frac{1}{2}},\quad d_3=\frac{\Sigma nd^3}{\Sigma nd^2},$$
$$Ud_3=\frac{\Sigma w}{\Sigma w/d_3},\quad D=\left(\frac{\Sigma nd^2}{\Sigma n}\right)^{\frac{1}{2}},\quad UD=\left(\frac{\Sigma w}{\Sigma w/D^3}\right)^{\frac{1}{2}},\quad d_4=\frac{\Sigma nd^4}{\Sigma nd^3},\quad Ud_4=\frac{\Sigma d_4 w}{\Sigma w}.$$

SAMPLE	MIXTURE OF	S	$N\times10^{10}$	d_1	Ud_1	Δ	U	d_3	Ud_3	D	UD	d_4	Ud_4
A		5.08	3975	0.132	1.39	0.143	1.55	0.21	1.48	0.165	1.64	0.27	1.25
B	single	2.36	448	.256	1.16	.314	1.42	.45	1.29	.342	1.38	.53	1.20
C	pigments	1.57	107	.44	1.36	.50	1.45	.675	1.4	.55	1.50	.77	1.345
D		.55	4.5	1.28	1.40	1.44	1.53	1.92	1.49	1.59	1.65	2.22	1.385
E	*A*+*B*	3.64	2013	.147	1.12	.173	1.21	.298	1.3	.207	1.36	.36	1.54
F	*A*+*C*	3.64	2420	.138	1.15	.160	1.27	.293	1.56	.196	1.43	.476	1.31
G	*A*+*D*	3.64	2720	.133	1.28	.150	1.43	.293	1.51	.187	1.60	.89	.985
H	*A*+*C*	3.30	2014	.140	1.09	.165	1.22	.322	1.35	.207	1.37	.52	1.215
I	*A*+*D*	2.84	2013	.133	1.18	.154	1.33	.374	1.32	.207	1.51	1.23	.90
M	*B*+*D*	1.57	255	.187	1.01	.226	1.10	.392	1.21	.272	1.23	.50	1.2
N	*A*+*B*+*D*	1.57	606	.162	.87	.208	1.00	.467	1.14	.272	1.14	.67	1.11
L'	*A*+*D*	1.57	890	.136	.91	.172	1.06	.683	.98	.292	1.23	1.79	.74
J	*A*+*B*	2.70	890	.270	1.02	.323	.955	.693	1.35	.292	.93	1.27	1.11
K	*A*+*C*	2.27	890	.161	.84	.209	.985	.680	1.08	.309	1.13	1.55	.875

gram may be calculated, Δ is the diameter of the particle of average surface and d_4 the diameter of the particle of average weight. The uniformity coefficients U, were calculated from the following equation given by Green:

$$U=d_1(\sum n/2\sum n(d_1-d)^2)^{\frac{1}{2}},$$

in which d_1 is any average diameter and is introduced to make U independent of magnification and dependent upon the relative values of particle size and the sum of the squares of the "residuals," $n(d_1-d)^2$. When all the particles are equal in size, U becomes infinite and the average diameters coincide. For mixtures the equation is expressed as a function of the fractional weight (W):

$$\bar{U}=\bar{d}\left(\Sigma\frac{w}{D^3}\Big/\Sigma\left\{\frac{w}{D^3}\left[\frac{d^2}{U^2}+2(\bar{d}-d)^2\right]\right\}\right)^{\frac{1}{2}}.$$

$\bar{d}$ is used to designate any fixed diameter of the mixture.

An inspection of Table I shows that the d_1 and Δ diameters have little significance in this instance, as for example sample I which is a 50.6 : 49.4 mixture of sample A (d_1= : 132; Δ=0.143) and sample D (d_1=1.28; Δ=1.44) has a d_1 diameter of 0.133 and a Δ diameter of 0.154. These diameters are actually smaller for sample I than for sample H which is a 49.3 : 50.7 mixture of samples A and C. The reason is that these diameters are so markedly affected by the fine particles and not appreciably by the coarse. Further, the values of the uniformity coefficients of the various mixtures are not in agreement with the uniformity which would be expected from the particle sizes of the components of the mixture. The agreement is satisfactory when the coefficient is calculated on the d_4 diameter and the next best results are obtained when the d_3 diameter is used, yet even in this case samples $G(A+D)$, and $F(A+C)$ appear more uniform than sample $E(A+B)$.

Lack of space makes it impossible to present all the data obtained on the properties of these pigments in rubber compounds but Figs. 10, 11 and 12 show some of the results obtained in a rather unusual test which measures principally the flow properties of the compounds. The formula used was as follows:

Smoked sheet	100
Sulphur	4
Diphenylguanidine	2
Zinc oxide	30 Vol.

These results were obtained with a pendulum which has been described elsewhere[7] and which measures: (a) resilience, or the percentage of the impact energy returned to the pendulum by the

[7] Barnett and Mathews, Ind. Eng. Chem. **26**, 1292 (1934).

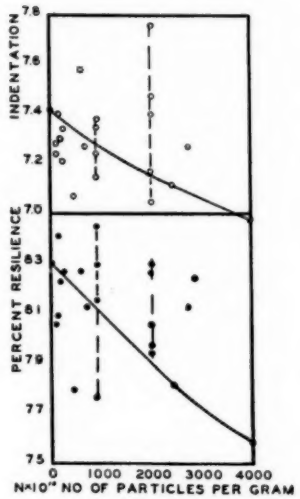

FIG. 10. Resilience and indentation *vs.* number of particles per gram.

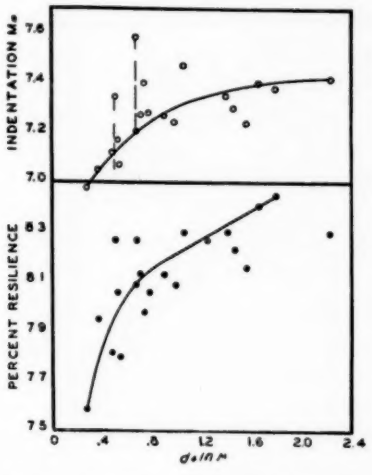

FIG. 12. Resilience and indentation *vs.* diameter (d_4) of particles.

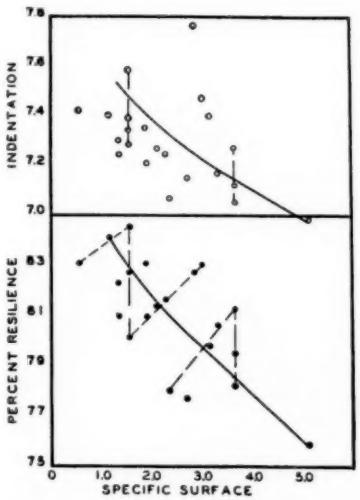

FIG. 11. Resilience and indentation *vs.* specific surface of particles.

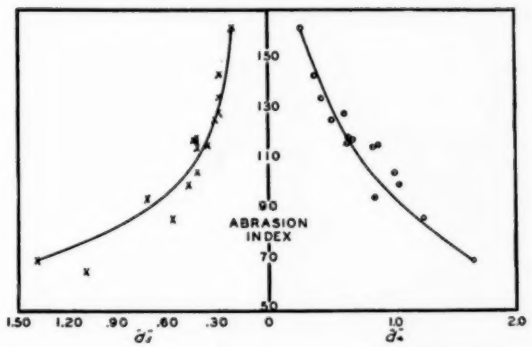

FIG. 13. Abrasion index *vs.* diameters d_3 and d_4.

rubber and (b) indentation, the depth of penetration of the hammer-shaped head of the pendulum into the sample. Figs. 10, 11 and 12 show the results for resilience and indentation plotted against the number of particles per gram, the specific surface and the d_4 diameter, respectively; the optimum cure for resilience was used in each case.

The agreement between the particle size measurements and the physical properties is obviously better in the last two cases than in the first and the agreement with the d_4 diameter seems somewhat better than with specific surface. The spread between samples having the same d_4 diameter is as great as between those having the same surface but in the specific surface curve there are definitely three groups of samples which if viewed independently would result in the conclusion that resilience and indentation increased with increasing specific surface, a conclusion not warranted in view of the data as a whole.

In Fig. 13, the data given by Haslam comparing the abrasion index with specific surface have been recalculated to show a comparison of this property with the d_3 and d_4 diameters. The d_4 diameter seems to give a somewhat better agreement with the physical property than does the d_3 diameter or the specific surface calculated from it. For instance, the series of pigments at constant surfaces show a definite trend in size as

indicated by the d_4 diameter which is in line with the abrasion index.

Perrot and Kinney in their discussion of the various average diameters have given a partial explanation of these results. They believe that the d_3 average diameter is the logical one to apply to paint pigments and fillers since the uniformity of the materials is so high that very little error is introduced. "Consider, however, the pigment 'ranging from ultramicroscopic particles to grains as coarse as sand.' The specific surface of such a pigment would be considerably less than the specific surface indicated by the average diameter, because the relative surfaces of the particles per unit weight of material have been neglected in calculation of this value." It seems very probable that the range of sizes in these synthetic mixtures of pigments involves this error. A number of investigators have endeavored to determine the effect of blending pigments. Dawson[8] reports that neither combinations of clay and carbon black nor of two zinc oxides follow the mixture law in tensile properties, or hysteresis, either in extension or rebound tests. Lefcaditis and Cotton[9] found a departure from the mixture law but in the opposite direction while Beaver and McKay[10] who also worked with clay and carbon black obtained values in concordance with the mixture law. If it were possible to measure the proper average diameters of these pigments in the state of dispersion existing in the rubber compounds, it might be possible to explain some of these apparent discrepancies.

[8] Dawson, Trans. I.R.I. **2**, 92 (1926).
[9] Lefcaditis and Cotton, Trans. I.R.I. **8**, 364 (1932).
[10] Beaver and McKay, Ind. Eng. Chem. **23**, 294 (1931).

Force at a Point in the Interior of a Semi-Infinite Solid

RAYMOND D. MINDLIN, *Department of Civil Engineering, Columbia University*

(Received March 13, 1936)

A solution of the three-dimensional elasticity equations for a homogeneous isotropic solid is given for the case of a concentrated force acting in the interior of a semi-infinite solid. This represents the fundamental solution having a singular point in a solid bounded by a plane. From it may be derived, by a known method of synthesis, the solutions for the semi-infinite solid which correspond to the solutions known as nuclei of strain in the solid of indefinite extent.

1. INTRODUCTION

ONE of the fundamental results in the theory of elasticity is the Kelvin solution[1] for a force applied at a point in a solid of indefinite extent. It is well known that stress distributions for a number of problems of practical importance may be obtained from the Kelvin solution by methods of synthesis and superposition.[2] For example, the problem, first solved by Lamé, of the stresses in a spherical container under uniform internal or external pressure may be treated by superposing stresses derived from Kelvin's results. First we form, from the Kelvin single force solution, the stresses for a double force, that is, a pair of equal and opposite forces acting at neighboring points. By superposing three mutually perpendicular double forces, we arrive at the solution known as the center of compression. Finally, the addition of a uniform tension or pressure to the center of compression leads to the solution of Lamé's problem.

The classical problem of Boussinesq dealing with a normal force applied at the plane boundary of a semi-infinite solid[3] has found practical application in the study of the distribution of foundation pressures, contact stresses, and in certain problems of soil mechanics. It is known that Boussinesq's problem may also be solved by superposing solutions derived from Kelvin's results. To do this we form a line of centers of compression by integrating the stresses for a single center of compression. By combining this result with the original Kelvin single-force solution, the Boussinesq formulas are obtained.

The Kelvin solution may be used in studying stresses due to a force applied at a great distance from a boundary while the Boussinesq solution is applicable in the case where the force acts at the surface. The solutions described in this paper fill in the gap between the two by giving the stresses for the case where the force is applied near the surface. Such a condition is approached in a number of practical problems such, for example, as in the case of a guy wire anchor. Again, by integrating these new solutions along a line, we may approximate the conditions produced by a friction pile or an anchor rod.

Solutions of the elasticity equations such as the single force, double force, center of compression, and line of centers of compression are referred to as nuclei of strain.[2] The number of nuclei of strain which may be obtained by synthesis from the Kelvin solution is unlimited and further combinations lead to the solutions for such important cases as Southwell's problem of the spherical cavity in an unlimited solid under simple tension[4] and Cerruti's problem of a force applied tangentially at the plane boundary of a semi-infinite solid.[5]

Each of the nuclei of strain obtained from Kelvin's results is a solution applicable to a solid of indefinite extent. With the solution for a force in the interior of a semi-infinite solid, as described in this paper, we may apply the method of synthesis to develop a new series of nuclei of strain for which the stresses vanish on the plane boundary of the semi-infinite solid. Such solutions may be termed half-space nuclei of strain.

[1] Sir W. Thomson, Cambridge and Dublin Math. J. (1848). See also A. E. H. Love, *Mathematical Theory of Elasticity*, fourth edition (Cambridge, 1927), p. 183; and S. Timoshenko, *Theory of Elasticity* (New York, 1934), p. 321.

[2] Love, p. 186, and Timoshenko, p. 323.

[3] J. Boussinesq, *Applications des Potentials* . . . (Paris, 1885). Also Love, p. 191, and Timoshenko, p. 331.

[4] R. V. Southwell and H. J. Gough, Phil. Mag. **1**, 71 (1926).

[5] V. Cerruti, Acc. Lincei. Mem. fis. mat., Roma **13**, 81 (1882). Also Love, p. 241.

The notion of such half-space nuclei of strain suggests some interesting possibilities. By employing these half-space nuclei as unit solutions, it may be possible to find solutions analogous to those obtained from the Kelvin nuclei but with the additional feature that a new plane boundary is introduced. For example, the solution analogous to Southwell's problem would pertain to a spherical cavity near the surface of a semi-infinite solid; the solution analogous to the problem of Boussinesq would be that for a force applied at the surface of a body bounded by two perpendicular planes (i.e., the transmission of force through "quarter-space"); the solution analogous to the hollow sphere under uniform pressure would apply to an eccentrically hollow sphere.

The present paper deals with the fundamental solution for the single force in the interior of a semi-infinite solid. The problem is divided into two parts: (1) force normal to the boundary; (2) force parallel to the boundary.

The discovery of the solutions followed a study of H. M. Westergaard's interpretation[6] of the problems of Kelvin, Boussinesq and Cerruti in terms of Galerkin vectors and the results obtained are shown to include these problems for certain limiting conditions.

2. The Galerkin Vector

The components of stress in an elastic isotropic solid were expressed by B. Galerkin[7] in terms of partial differential coefficients of three functions satisfying a fourth-order equation. P. F. Papkovitch[8] and H. M. Westergaard[9] have expressed the displacements and stresses in terms of a vector stress function whose scalar coefficients are the Galerkin functions. The displacements are given, in Westergaard's form of the Galerkin vector, by[9]

$$\begin{aligned} u &= (1/2G)[2(1-\mu)\Delta X - (\partial/\partial x)\ \mathrm{div}\ \mathbf{F}], \\ v &= (1/2G)[2(1-\mu)\Delta Y - (\partial/\partial y)\ \mathrm{div}\ \mathbf{F}], \\ w &= (1/2G)[2(1-\mu)\Delta Z - (\partial/\partial z)\ \mathrm{div}\ \mathbf{F}], \end{aligned} \tag{1}$$

where: X, Y, Z are the Galerkin functions,
$\mathbf{i}$, $\mathbf{j}$, $\mathbf{k}$ constitute an orthogonal system of unit vectors
$\mathbf{F} = \mathbf{i}X + \mathbf{j}Y + \mathbf{k}Z$ is the Galerkin vector,
Δ is Laplace's operator,
G is the modulus of rigidity,
μ is Poisson's ratio.

The stresses are given by[9]

$$\begin{aligned} \sigma_x &= 2(1-\mu)\partial\Delta X/\partial x + (\mu\Delta - \partial^2/\partial x^2)\ \mathrm{div}\ \mathbf{F}, \\ \sigma_y &= 2(1-\mu)\partial\Delta Y/\partial y + (\mu\Delta - \partial^2/\partial y^2)\ \mathrm{div}\ \mathbf{F}, \\ \sigma_z &= 2(1-\mu)\partial\Delta Z/\partial z + (\mu\Delta - \partial^2/\partial z^2)\ \mathrm{div}\ \mathbf{F}, \\ \tau_{yz} &= (1-\mu)(\partial\Delta Y/\partial z + \partial\Delta Z/\partial y) \\ &\qquad - (\partial^2/\partial y\partial z)\ \mathrm{div}\ \mathbf{F}, \\ \tau_{zx} &= (1-\mu)(\partial\Delta Z/\partial x + \partial\Delta X/\partial z) \\ &\qquad - (\partial^2/\partial z\partial x)\ \mathrm{div}\ \mathbf{F}, \\ \tau_{xy} &= (1-\mu)(\partial\Delta X/\partial y + \partial\Delta Y/\partial x) \\ &\qquad - (\partial^2/\partial x\partial y)\ \mathrm{div}\ \mathbf{F}. \end{aligned} \tag{2}$$

For the case of zero body force, the Galerkin vector must satisfy the biharmonic equation,

$$\Delta^2\mathbf{F} = 0. \tag{3}$$

It was observed by Professor Westergaard[6] that the coefficient of a single axially symmetrical component of the Galerkin vector is identical with Love's function[10] for strain symmetrical about the corresponding axis.

3. Nuclei of Strain in Terms of Galerkin Vectors

The solutions given in sections 4 and 5 were obtained by superposition of nuclei of strain for an unlimited solid. It has been found convenient, in applying the method of superposition, to express the nuclei of strain in terms of Galerkin vectors.

In the following list of functions, A, B, C, $\cdots$ H are constants and $R = (x^2+y^2+z^2)^{\frac{1}{2}}$. It may be observed that each of the functions satisfies the biharmonic equation and that the stresses derived from them vanish at infinity.

[6] H. M. Westergaard, *Lectures on Elasticity while Visiting Professor at the University of Michigan* (Summer Session, 1934).
[7] B. Galerkin, Comptes rendus **190**, 1047 (1930).
[8] P. F. Papkovitch, Comptes rendus **195**, 513, 754 (1932).
[9] H. M. Westergaard, Bull. Am. Math. Soc. **41**, 695 (1935).
[10] Love, p. 274; Timoshenko, p. 309.

GALERKIN VECTORS FOR NUCLEI OF STRAIN IN AN UNLIMITED SOLID

A. Single force (Kelvin's problem).

(1) $\mathbf{i}AR$ (single force in x direction)
(2) $\mathbf{j}AR$ (single force in y direction)
(3) $\mathbf{k}AR$ (single force in z direction)

B. Double force

(1) $\mathbf{i}Bx/R$ (double force in x direction)
(2) $\mathbf{j}By/R$ (double force in y direction)
(3) $\mathbf{k}Bz/R$ (double force in z direction)

C. Double force with moment

(1) $\mathbf{i}Cz/R$ (double force in x direction with moment about y axis)
(2) $\mathbf{j}Cx/R$ (double force in y direction with moment about z axis)
(3) $\mathbf{k}Cy/R$ (double force in z direction with moment about x axis)
(4) $\mathbf{i}Cy/R$ (double force in x direction with moment about z axis)
(5) $\mathbf{j}Cz/R$ (double force in y direction with moment about x axis)
(6) $\mathbf{k}Cx/R$ (double force in z direction with moment about y axis)

D. Line of double forces with moment

(1) $\mathbf{i}Dz \log (R+x)$ (type $C(1)$ along x axis from $x=0$ to $x=-\infty$)
(2) $\mathbf{j}Dx \log (R+y)$ (type $C(2)$ along y axis from $y=0$ to $y=-\infty$)
(3) $\mathbf{k}Dy \log (R+z)$ (type $C(3)$ along z axis from $z=0$ to $z=-\infty$)
(4) $\mathbf{i}Dy \log (R+x)$ (type $C(4)$ along x axis from $x=0$ to $x=-\infty$)
(5) $\mathbf{j}Dz \log (R+y)$ (type $C(5)$ along y axis from $y=0$ to $y=-\infty$)
(6) $\mathbf{k}Dx \log (R+z)$ (type $C(6)$ along z axis from $z=0$ to $z=-\infty$)

E. Center of compression or dilatation

(1) $\mathbf{i}E \log (R+x)$
(2) $\mathbf{j}E \log (R+y)$ (All three yield the same stresses)
(3) $\mathbf{k}E \log (R+z)$

F. Line of compression or dilatation of constant strength

(1) $\mathbf{i}F[x \log (R+x)-R]$ (along x axis from $x=0$ to $x=-\infty$)
(2) $\mathbf{j}F[y \log (R+y)-R]$ (along y axis from $y=0$ to $y=-\infty$)
(3) $\mathbf{k}F[z \log (R+z)-R]$ (along z axis from $z=0$ to $z=-\infty$)

G. Doublet (double center of compression-dilatation)

(1) $\mathbf{i}G(1/R)$ (axis of doublet parallel to x axis)
(2) $\mathbf{j}G(1/R)$ (axis of doublet parallel to y axis)
(3) $\mathbf{k}G(1/R)$ (axis of doublet parallel to z axis)

H. Linearly varying line of doublets with strength proportional to distance from the origin

(1) $\mathbf{i}H[z \log (R+z)-R]$ (type $G(1)$ along z axis from $z=0$ to $z=-\infty$)
(2) $\mathbf{j}H[x \log (R+x)-R]$ (type $G(2)$ along x axis from $x=0$ to $x=-\infty$)
(3) $\mathbf{k}H[y \log (R+y)-R]$ (type $G(3)$ along y axis from $y=0$ to $y=-\infty$)
(4) $\mathbf{i}H[y \log (R+y)-R]$ (type $G(1)$ along y axis from $y=0$ to $y=-\infty$)
(5) $\mathbf{j}H[z \log (R+z)-R]$ (type $G(2)$ along z axis from $z=0$ to $z=-\infty$)
(6) $\mathbf{k}H[x \log (R+x)-R]$ (type $G(3)$ along x axis from $x=0$ to $x=-\infty$)

4. FORCE NORMAL TO THE BOUNDARY OF A SEMI-INFINITE SOLID

The semi-infinite solid is considered to be bounded by the plane $z=0$, the positive z axis penetrating into the body. A force P is applied at point $(0, 0, +c)$ and acts in the positive z direction (Fig. 1).

Since the stress will be symmetrical about the z axis, we need consider only the $\mathbf{k}$ component of $\mathbf{F}$. Transforming to cylindrical coordinates r, θ, z and noting that Z is independent of θ, we find, from Eqs. (1) and (2), the following expressions for the displacements and stresses in symmetrical cylindrical coordinates:[10]

$$
\begin{aligned}
U &= -(1/2G)(\partial^2 Z/\partial r \partial z), \\
w &= (1/2G)[2(1-\mu)\Delta Z - \partial^2 Z/\partial z^2], \\
\sigma_r &= (\partial/\partial z)[\mu \Delta Z - \partial^2 Z/\partial r^2], \\
\sigma_\theta &= (\partial/\partial z)[\mu \Delta Z - (1/r)(\partial Z/\partial r)], \\
\sigma_z &= (\partial/\partial z)[(2-\mu)\Delta Z - \partial^2 Z/\partial z^2], \\
\tau_{rz} &= (\partial/\partial r)[(1-\mu)\Delta Z - \partial^2 Z/\partial z^2].
\end{aligned}
\tag{4}
$$

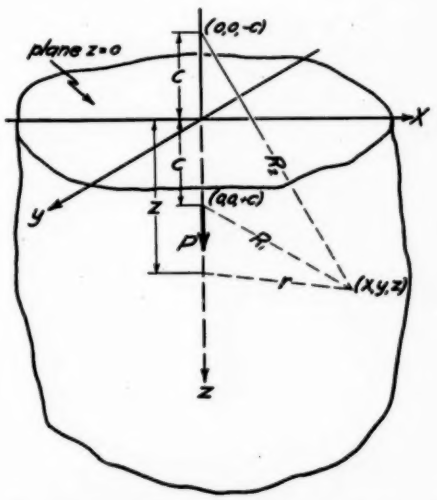

FIG. 1. Force normal to the boundary in the interior of a semi-infinite solid.

We first apply the Kelvin solution at point $(0, 0, +c)$ by replacing R with $R_1=(r^2+(z-c)^2)^{\frac{1}{2}}$ in solution $A(3)$ of section 3. We note that stresses σ_z and τ_{rz} are produced on the plane $z=0$. The boundary conditions for $z=0$ are

$$[\sigma_z]_{z=0}=[\tau_{rz}]_{z=0}=0. \tag{5}$$

It is therefore necessary to add further solutions to remove the boundary stresses and these solutions must introduce no new singularities in the region $z\geqq 0$. Nuclei of strain of types $A(3)$, $B(3)$, $E(3)$, $F(3)$ and $G(3)$, applied at $(0, 0, -c)$, are found to satisfy these conditions if the proper values are assigned to the constants A, B, E, F and G.

To transfer nuclei of strain from the origin to $(0, 0, -c)$, we replace z with $(z+c)$ and R with $R_2=(r^2+(z+c)^2)^{\frac{1}{2}}$ in the formulas of section 3.

The values of the constants are obtained from the boundary Eqs. (5) and the equilibrium condition

$$P=-\int_0^\infty 2\pi r\sigma_z dr, \quad (z>c). \tag{6}$$

This procedure leads us to the required Galerkin vector:

$$\mathbf{F}=[P\mathbf{k}/8\pi(1-\mu)]\{R_1+(3-4\mu)R_2-2c(z+c)/R_2-4(1-2\mu)c\log(R_2+z+c)$$
$$+4(1-\mu)(1-2\mu)[(z+c)\log(R_2+z+c)-R_2]+2c^2/R_2\}. \tag{7}$$

The solution for a force in the interior of a semi-infinite solid and normal to the boundary is seen to be compounded of six nuclei of strain which, in an unlimited solid, represent: (1) a single force at $(0, 0, +c)$; (2) a single force at $(0, 0, -c)$; (3) a double force at $(0, 0, -c)$; (4) a center of compression at $(0, 0, -c)$; (5) a line of centers of compression extending from $z=-c$ to $z=-\infty$; (6) a doublet at $(0, 0, -c)$.

Collecting terms in Eq. (7) we obtain:[11]

$$\mathbf{F}=[P\mathbf{k}/8\pi(1-\mu)]\{R_1+[8\mu(1-\mu)-1]R_2+4(1-2\mu)[(1-\mu)z-\mu c]\log(R_2+z+c)-2cz/R_2\}. \tag{8}$$

Eqs. (8) and (4) yield the displacements and stresses:

$$U=\frac{Pr}{16\pi G(1-\mu)}\left[\frac{z-c}{R_1^3}+\frac{(3-4\mu)(z-c)}{R_2^3}-\frac{4(1-\mu)(1-2\mu)}{R_2(R_2+z+c)}+\frac{6cz(z+c)}{R_2^5}\right],$$

$$w=\frac{P}{16\pi G(1-\mu)}\left[\frac{3-4\mu}{R_1}+\frac{8(1-\mu)^2-(3-4\mu)}{R_2}+\frac{(z-c)^2}{R_1^3}+\frac{(3-4\mu)(z+c)^2-2cz}{R_2^3}+\frac{6cz(z+c)^2}{R_2^5}\right],$$

$$\sigma_r=\frac{P}{8\pi(1-\mu)}\left[\frac{(1-2\mu)(z-c)}{R_1^3}-\frac{(1-2\mu)(z+7c)}{R_2^3}+\frac{4(1-\mu)(1-2\mu)}{R_2(R_2+z+c)}-\frac{3r^2(z-c)}{R_1^5}\right.$$
$$\left.+\frac{6c(1-2\mu)(z+c)^2-6c^2(z+c)-3(3-4\mu)r^2(z-c)}{R_2^5}-\frac{30cr^2z(z+c)}{R_2^7}\right], \tag{9}$$

$$\sigma_\theta=\frac{P(1-2\mu)}{8\pi(1-\mu)}\left[\frac{(z-c)}{R_1^3}+\frac{(3-4\mu)(z+c)-6c}{R_2^3}-\frac{4(1-\mu)}{R_2(R_2+z+c)}+\frac{6c(z+c)^2}{R_2^5}-\frac{6c^2(z+c)}{(1-2\mu)R_2^5}\right],$$

$$\sigma_z=\frac{P}{8\pi(1-\mu)}\left[-\frac{(1-2\mu)(z-c)}{R_1^3}+\frac{(1-2\mu)(z-c)}{R_2^3}-\frac{3(z-c)^3}{R_1^5}\right.$$
$$\left.-\frac{3(3-4\mu)z(z+c)^2-3c(z+c)(5z-c)}{R_2^5}-\frac{30cz(z+c)^3}{R_2^7}\right],$$

$$\tau_{rz}=\frac{Pr}{8\pi(1-\mu)}\left[-\frac{1-2\mu}{R_1^3}+\frac{1-2\mu}{R_2^3}-\frac{3(z-c)^2}{R_1^5}-\frac{3(3-4\mu)z(z+c)-3c(3z+c)}{R_2^5}-\frac{30cz(z+c)^2}{R_2^7}\right].$$

[11] R. D. Mindlin, Comptes rendus **201**, 536 (1935).

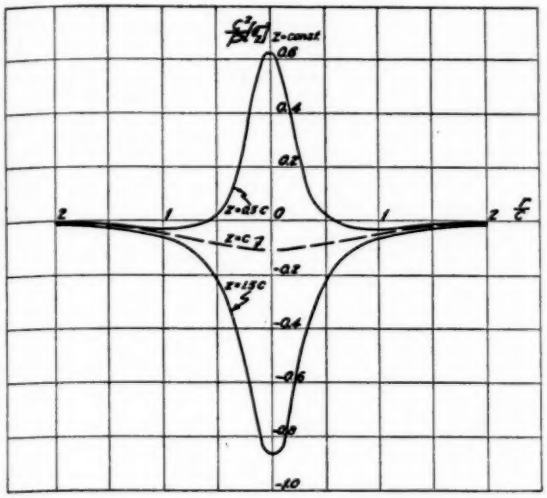

FIG. 2. Normal stress on planes parallel to boundary for the case of a force normal to the boundary ($\mu=0.3$).

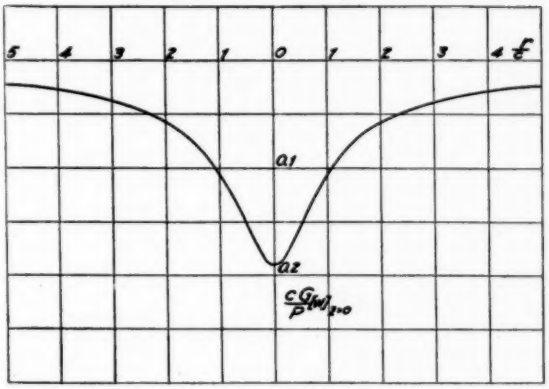

FIG. 3. Vertical deflection of the surface for the case of a force normal to the boundary ($\mu=0.3$).

Fig. 2 shows the distribution of normal stress on horizontal planes, and Fig. 3 shows the vertical deflection of the surface of the semi-infinite solid.

When $c\rightarrow\infty$ all terms in Eqs. (9) containing R_2 vanish and the solution becomes that for Kelvin's problem where the force is applied at $(0, 0, +c)$ in the positive z direction. The corresponding Galerkin vector is

$$\mathbf{F}=\mathbf{k}[PR_1/8\pi(1-\mu)]. \tag{10}$$

When $c\rightarrow 0$ Eqs. (9) give the stresses and displacements for Boussinesq's problem.[12] These stresses are represented by the Galerkin vector

$$\mathbf{F}=\mathbf{k}(P/2\pi)[2\mu R+(1-2\mu)z\log(R+z)]. \tag{11}$$

The solution for the problem of Boussinesq was given by Professor Westergaard[6] in the form of the Galerkin vector

$$\mathbf{F}=\mathbf{k}(PR/2\pi) \tag{12a}$$

combined with the potential function

$$\phi=-[(1-2\mu)/2\pi]P\log(R+z). \tag{12b}$$

The relation between ϕ and $\mathbf{F}$ is given by

$$\text{grad }\phi=2(1-\mu)\Delta\mathbf{F}-\text{grad div }\mathbf{F}. \tag{13}$$

As a further verification of the solution, we may compare the stresses with those obtained for the corresponding two-dimensional case by E. Melan.[13] While the approach to the solution in three dimensions was simplified through the use of cylindrical coordinates, the comparison with Melan's formulas is facilitated by referring the components of stress to rectangular coordinates. Eqs. (9) then become:

[12] The stresses and displacements for the problems of Boussinesq and Cerruti are given by F. Vogt, *Det Norske Videnskaps Akademi i Oslo*, Math.-Naturv. klasse, No. 2, pp. 5, 20 (1925).

[13] E. Melan, Zeits. f. angew. Math. und Mech. **12**, 343 (1932). This comparison was suggested by Professor S. Timoshenko.

$$\sigma_x=\frac{P}{8\pi(1-\mu)}\left[\frac{(1-2\mu)(z-c)}{R_1^3}-\frac{3x^2(z-c)}{R_1^5}+\frac{(1-2\mu)[3(z-c)-4\mu(z+c)]}{R_2^3}\right.$$
$$-\frac{3(3-4\mu)x^2(z-c)-6c(z+c)[(1-2\mu)z-2\mu c]}{R_2^5}-\frac{30cx^2z(z+c)}{R_2^7}$$
$$\left.-\frac{4(1-\mu)(1-2\mu)}{R_2(R_2+z+c)}\left(1-\frac{x^2}{R_2(R_2+z+c)}-\frac{x^2}{R_2^2}\right)\right],$$

$$\sigma_y=\frac{P}{8\pi(1-\mu)}\left[\frac{(1-2\mu)(z-c)}{R_1^3}-\frac{3y^2(z-c)}{R_1^5}+\frac{(1-2\mu)[3(z-c)-4\mu(z+c)]}{R_2^3}\right.$$
$$-\frac{3(3-4\mu)y^2(z-c)-6c(z+c)[(1-2\mu)z-2\mu c]}{R_2^5}-\frac{30cy^2z(z+c)}{R_2^7}$$
$$\left.-\frac{4(1-\mu)(1-2\mu)}{R_2(R_2+z+c)}\left(1-\frac{y^2}{R_2(R_2+z+c)}-\frac{y^2}{R_2^2}\right)\right], \quad (14)$$

$$\sigma_z=\frac{P}{8\pi(1-\mu)}\left[-\frac{(1-2\mu)(z-c)}{R_1^3}+\frac{(1-2\mu)(z-c)}{R_2^3}-\frac{3(z-c)^3}{R_1^5}\right.$$
$$\left.-\frac{3(3-4\mu)z(z+c)^2-3c(z+c)(5z-c)}{R_2^5}-\frac{30cz(z+c)^3}{R_2^7}\right],$$

$$\tau_{yz}=\frac{Py}{8\pi(1-\mu)}\left[-\frac{(1-2\mu)}{R_1^3}+\frac{(1-2\mu)}{R_2^3}-\frac{3(z-c)^2}{R_1^5}-\frac{3(3-4\mu)z(z+c)-3c(3z+c)}{R_2^5}-\frac{30cz(z+c)^2}{R_2^7}\right],$$

$$\tau_{zx}=\frac{Px}{8\pi(1-\mu)}\left[-\frac{(1-2\mu)}{R_1^3}+\frac{(1-2\mu)}{R_2^3}-\frac{3(z-c)^2}{R_1^5}-\frac{3(3-4\mu)z(z+c)-3c(3z+c)}{R_2^5}-\frac{30cz(z+c)^2}{R_2^7}\right],$$

$$\tau_{xy}=\frac{Pxy}{8\pi(1-\mu)}\left[-\frac{3(z-c)}{R_1^5}-\frac{3(3-4\mu)(z-c)}{R_2^5}+\frac{4(1-\mu)(1-2\mu)}{R_2^2(R_2+z+c)}\left(\frac{1}{R_2+z+c}+\frac{1}{R_2}\right)-\frac{30cz(z+c)}{R_2^7}\right].$$

We consider a uniform distribution of forces of magnitude p per unit of length along a line through $(0, 0, +c)$ parallel to the y axis. If db is a small element of this line at a distance b from the z axis, the stresses due to the uniform pressure p acting on db are found by substituting pdb for P and $(y-b)$ for y in Eqs. (14). If, now, we integrate these formulas with respect to b between the limits $-\infty$ and $+\infty$, we obtain the corresponding solution for plane strain. By taking account of the relations between the elastic constants for plane strain and plane stress and also noting an interchange of axes, this procedure leads directly to the stresses given by Melan.

5. Force Parallel to the Boundary of a Semi-Infinite Solid

In this case there is no axial symmetry and we employ rectangular coordinates (x, y, z), and Eqs. (1) and (2). The force P is applied at $(0, 0, +c)$ and acts in the positive x direction (Fig. 4).

We again begin by applying the Kelvin solution at $(0, 0, +c)$, this time using type $A(1)$. To remove the stresses on plane $z=0$, introduced by the single force, we employ nuclei of strain of types $A(1)$, $C(6)$, $D(6)$, $G(1)$ and $H(1)$, again substituting $(z+c)$ for z and $R_2=(x^2+y^2+(z+c)^2)^{\frac{1}{2}}$ for R. The constants associated with these solutions are determined from the boundary conditions $[\sigma_z]_{z=0}=[\tau_{yz}]_{z=0}=[\tau_{zx}]_{z=0}=0$ (15)

and the equilibrium condition

$$P=-4\int_0^\infty\int_0^\infty \tau_{zz}dydx, \quad (z>c). \tag{16}$$

The result of these operations is the Galerkin vector[11]

$$\mathbf{F}=[P/8\pi(1-\mu)](\mathbf{i}\{R_1+R_2-2c^2/R_2 +4(1-\mu)(1-2\mu)[(z+c)\log(R_2+z+c)-R_2]\} +\mathbf{k}\{2cx/R_2+2(1-2\mu)x\log(R_2+z+c)\}). \tag{17}$$

Thus, for the case of a force in the interior of a semi-infinite solid, parallel to the boundary, the solution is obtained by superposition of six nuclei of strain for the unlimited solid: (1) a single force at (0, 0, $+c$); (2) a single force at (0, 0, $-c$); (3) a doublet at (0, 0, $-c$); (4) a semi-infinite line of doublets extending from $z=-c$ to $z=-\infty$ with strength proportional to the distance from $z=-c$; (5) a double force with moment at (0, 0, $-c$); (6) a semi-infinite line of double forces with moment extending from $z=-c$ to $z=-\infty$.

The displacements and stresses, obtained from Eqs. (1), (2) and (17), are found to be:

$$u=\frac{P}{16\pi G(1-\mu)}\left[\frac{3-4\mu}{R_1}+\frac{1}{R_2}+\frac{x^2}{R_1^3}+\frac{(3-4\mu)x^2}{R_2^3}+\frac{2cz}{R_2^3}\left(1-\frac{3x^2}{R_2^2}\right)+\frac{4(1-\mu)(1-2\mu)}{R_2+z+c}\left(1-\frac{x^2}{R_2(R_2+z+c)}\right)\right],$$

$$v=\frac{Pxy}{16\pi G(1-\mu)}\left[\frac{1}{R_1^3}+\frac{3-4\mu}{R_2^3}-\frac{6cz}{R_2^5}-\frac{4(1-\mu)(1-2\mu)}{R_2(R_2+z+c)^2}\right],$$

$$w=\frac{Px}{16\pi G(1-\mu)}\left[\frac{z-c}{R_1^3}+\frac{(3-4\mu)(z-c)}{R_2^3}-\frac{6cz(z+c)}{R_2^5}+\frac{4(1-\mu)(1-2\mu)}{R_2(R_2+z+c)}\right],$$

$$\sigma_x=\frac{Px}{8\pi(1-\mu)}\left[-\frac{(1-2\mu)}{R_1^3}+\frac{(1-2\mu)(5-4\mu)}{R_2^3}-\frac{3x^2}{R_1^5}-\frac{3(3-4\mu)x^2}{R_2^5} -\frac{4(1-\mu)(1-2\mu)}{R_2(R_2+z+c)^2}\left(3-\frac{x^2(3R_2+z+c)}{R_2^2(R_2+z+c)}\right)+\frac{6c}{R_2^5}\left(3c-(3-2\mu)(z+c)+\frac{5x^2z}{R_2^2}\right)\right],$$

$$\sigma_y=\frac{Px}{8\pi(1-\mu)}\left[\frac{(1-2\mu)}{R_1^3}+\frac{(1-2\mu)(3-4\mu)}{R_2^3}-\frac{3y^2}{R_1^5}-\frac{3(3-4\mu)y^2}{R_2^5} -\frac{4(1-\mu)(1-2\mu)}{R_2(R_2+z+c)^2}\left(1-\frac{y^2(3R_2+z+c)}{R_2^2(R_2+z+c)}\right)+\frac{6c}{R_2^5}\left(c-(1-2\mu)(z+c)+\frac{5y^2z}{R_2^2}\right)\right], \tag{18}$$

$$\sigma_z=\frac{Px}{8\pi(1-\mu)}\left[\frac{(1-2\mu)}{R_1^3}-\frac{(1-2\mu)}{R_2^3}-\frac{3(z-c)^2}{R_1^5}-\frac{3(3-4\mu)(z+c)^2}{R_2^5}+\frac{6c}{R_2^5}\left(c+(1-2\mu)(z+c)+\frac{5z(z+c)^2}{R_2^2}\right)\right],$$

$$\tau_{yz}=\frac{Pxy}{8\pi(1-\mu)}\left[-\frac{3(z-c)}{R_1^5}-\frac{3(3-4\mu)(z+c)}{R_2^5}+\frac{6c}{R_2^5}\left(1-2\mu+\frac{5z(z+c)}{R_2^2}\right)\right],$$

$$\tau_{zz}=\frac{P}{8\pi(1-\mu)}\left[-\frac{(1-2\mu)(z-c)}{R_1^3}+\frac{(1-2\mu)(z-c)}{R_2^3}-\frac{3x^2(z-c)}{R_1^5}-\frac{3(3-4\mu)x^2(z+c)}{R_2^5} -\frac{6c}{R_2^5}\left(z(z+c)-(1-2\mu)x^2-\frac{5x^2z(z+c)}{R_2^2}\right)\right],$$

$$\tau_{xy}=\frac{Py}{8\pi(1-\mu)}\left[-\frac{(1-2\mu)}{R_1^3}+\frac{(1-2\mu)}{R_2^3}-\frac{3x^2}{R_1^5}-\frac{3(3-4\mu)x^2}{R_2^5} -\frac{4(1-\mu)(1-2\mu)}{R_2(R_2+z+c)^2}\left(1-\frac{x^2(3R_2+z+c)}{R_2^2(R_2+z+c)}\right)-\frac{6cz}{R_2^5}\left(1-\frac{5x^2}{R_2^2}\right)\right].$$

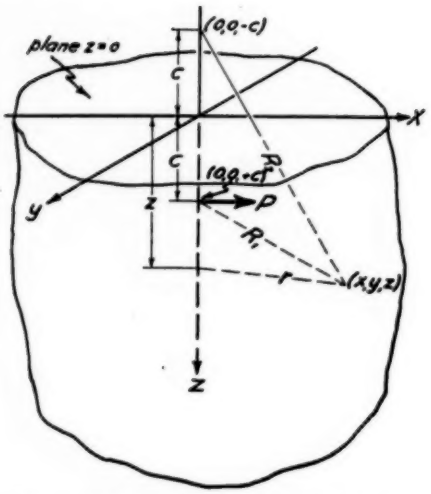

FIG. 4. Force parallel to the boundary in the interior of a semi-infinite solid.

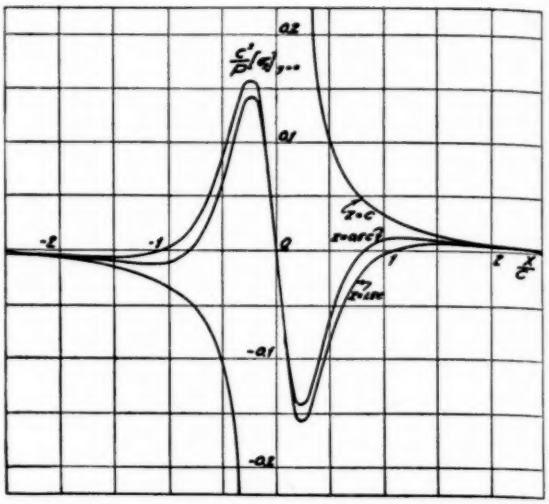

FIG. 5. Normal stress along lines parallel to the x axis on planes parallel to the boundary for the case of a force parallel to the boundary ($\mu=0.3$).

Fig. 5 shows the distribution of normal stress on horizontal planes, and Fig. 6 shows the vertical deflection of the surface of the solid along the x axis.

When $c\to\infty$ all terms in Eq. (18) containing R_2 vanish and the solution becomes that for Kelvin's problem with the force applied at $(0, 0, +c)$ in the positive x direction. The corresponding Galerkin vector is

$$\mathbf{F}=\mathbf{i}[PR_1/8\pi(1-\mu)]. \tag{19}$$

When $c\to 0$ Eqs. (18) give the stresses and displacements for the problem of Cerruti.[12] These results are represented by the Galerkin vector

$$\mathbf{F}=[P/4\pi(1-\mu)](\mathbf{i}\{R+2(1-\mu)(1-2\mu)\times[z\log(R+z)-R]\}+\mathbf{k}\{(1-2\mu)x\log(R+z)\}). \tag{20}$$

The solution for the problem of Cerruti was given by Professor Westergaard[6] in the form of the Galerkin vector

$$\mathbf{F}=[P/4\pi(1-\mu)][\mathbf{i}R+\mathbf{k}(1-2\mu)x\log(R+z)] \tag{21a}$$

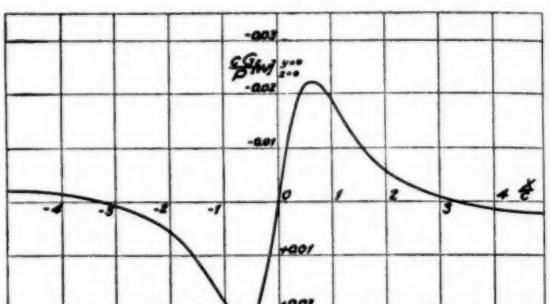

FIG. 6. Vertical deflection of the surface along the x axis for the case of a force parallel to the boundary ($\mu=0.3$).

combined with the potential function

$$\phi=[(1-2\mu)P/2\pi][x/(R+z)]. \tag{21b}$$

Following the same procedure as in the case of the normal force, the stresses given in Eqs. (18) may be reduced to Melan's formulas for the two-dimensional analog.[13]

The author is indebted to Professor H. M. Westergaard for valuable criticisms of the manuscript.